Volume 53
Number 26
14 July 2024
Pages 10757-11178

# Dalton Transactions

An international journal of inorganic chemistry

rsc.li/dalton

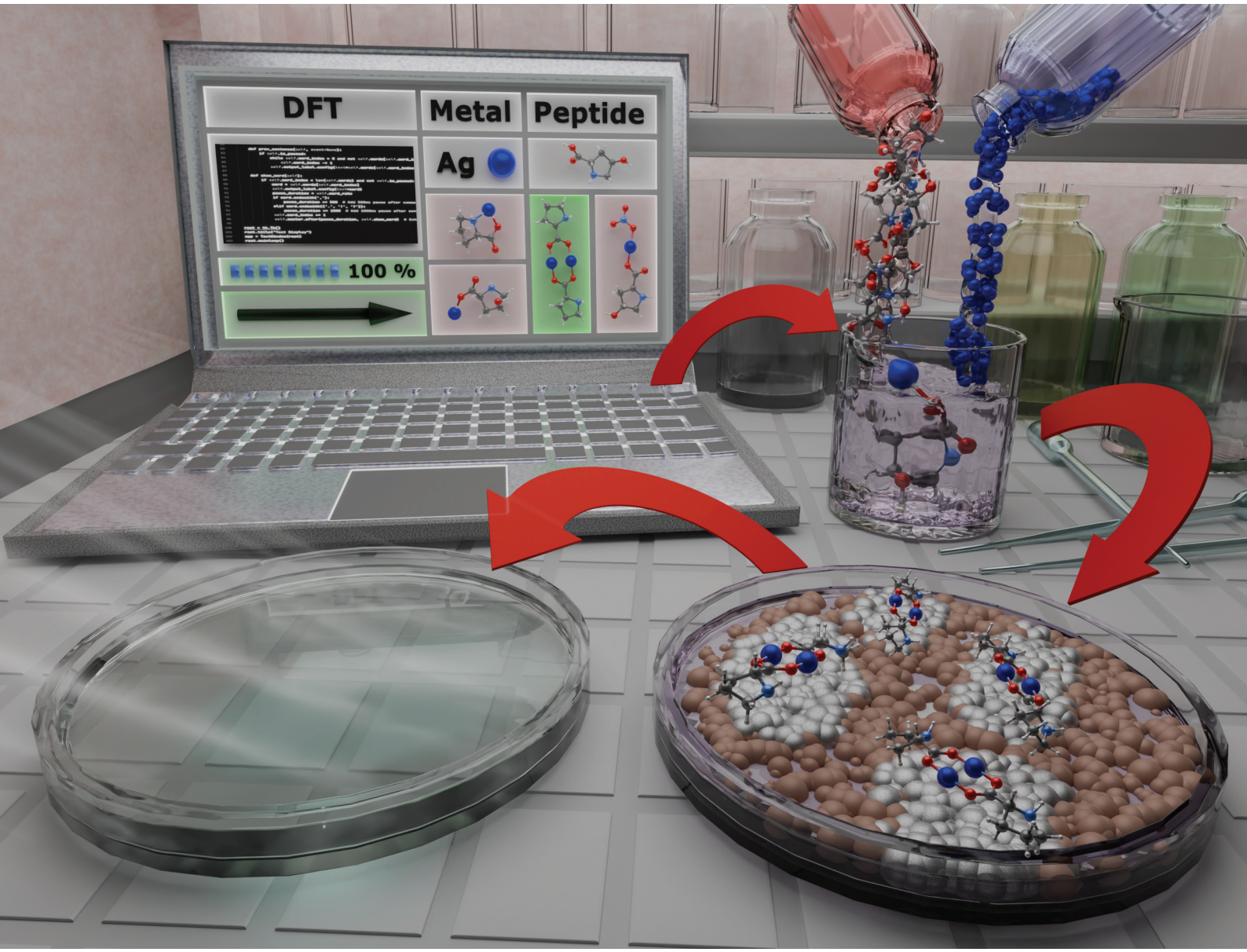


ISSN 1477-9226

ROYAL SOCIETY OF CHEMISTRY

**PAPER**

Zuzana Vargová *et al.*

Influence of proline and hydroxyproline as antimicrobial and anticancer peptide components on the silver(I) ion activity: structural and biological evaluation with a new theoretical and experimental SAR approach

Dalton Transactions

ROYAL SOCIETY OF CHEMISTRY

PAPER

View Article Online
View Journal | View Issue

Check for updates

Cite this: *Dalton Trans.*, 2024, **53**, 10834

Published on 12 April 2024. Downloaded on 3/12/2025 6:23:37 AM.

# Influence of proline and hydroxyproline as antimicrobial and anticancer peptide components on the silver(I) ion activity: structural and biological evaluation with a new theoretical and experimental SAR approach†

Gabriela Kuzderová,[a] Simona Sovová,[b,c] Michaela Rendošová,[a] Róbert Gyepes,[d] Danica Sabolová,[b] Ivona Kožárová,[c] Ľudmila Balážová,[e] Mária Vilková,[f] Martin Kello,[g] Alan Liška[h] and Zuzana Vargová *[a]

Silver(I) complexes with proline and hydroxyproline were synthesized and structurally characterized and crystal structure analysis shows that the formulas of the compounds are $\{[Ag_2(Pro)_2(NO_3)]NO_3\}_n$ (AgPro) (Pro = L-proline) and $\{[Ag_2(Hyp)_2(NO_3)]NO_3\}_n$ (AgHyp) (Hyp = *trans*-4-hydroxy-L-proline). Both complexes crystallize in the monoclinic lattice with space group $P2_1$ with a carboxylate bidentate-bridging coordination mode of the organic ligands Pro and Hyp (with $NH_2^+$ and $COO^-$ groups in zwitterionic form). Both complexes have a distorted seesaw ($C_{2v}$) geometry around one silver(I) ion with $\tau_4$ values of 58% (AgPro) and 51% (AgHyp). Moreover, the results of spectral and thermal analyses correlate with the structural ones. $^1H$ and $^{13}C$ NMR spectra confirm the complexes species' presence in the DMSO biological testing medium and their stability in the time range of the bioassays. In addition, molar conductivity measurements indicate complexes' behaviour like 1 : 1 electrolytes. Both complexes showed higher or the same antibacterial activity against *Bacillus cereus*, *Pseudomonas aeruginosa* and *Staphylococcus aureus* as $AgNO_3$ (MIC = 0.063 mM) and higher than silver(I) sulfadiazine (AgSD) (MIC > 0.5 mM) against *Pseudomonas aeruginosa*. In addition, complex AgPro exerted a strong cytotoxic effect against the tested MDA-MB-231 and Jurkat cancer cell lines ($IC_{50}$ values equal to 3.7 and 3.0 μM, respectively) compared with $AgNO_3$ ($IC_{50}$ = 6.1 (5.7) μM) and even significantly higher selectivity than cisplatin (cisPt) against MDA-MB-231 cancer cell lines (SI = 3.05 (AgPro); 1.16 (cisPt), SI – selectivity index). The binding constants and the number of binding sites ($n$) of AgPro and AgHyp complexes with bovine serum albumin (BSA) were determined at four different temperatures, and the zeta potential of BSA in the presence of silver(I) complexes was also measured. The *in ovo* method shows the safety of the topical and intravenous application of AgPro and AgHyp. Moreover, the complexes' bioavailability was verified by lipophilicity evaluation from the experimental and theoretical points of view.

Received 8th February 2024,
Accepted 10th April 2024

DOI: 10.1039/d4dt00389f

rsc.li/dalton

## Introduction

It is very well known that within the EU, the greatest mortality is caused by circulatory diseases, cancer, and infectious diseases (in recent years, COVID). To reduce this mortality, individual EU states (as well as the rest of the world) support research aimed at developing different types of therapy for these diseases. Chemotherapy is a frequently used method in

[a]*Department of Inorganic Chemistry, Faculty of Science, P.J.Šafárik University, Moyzesova 11, 041 54 Košice, Slovak Republic. E-mail: zuzana.vargova@upjs.sk*
[b]*Department of Biochemistry, Faculty of Science, P.J.Šafárik University, Moyzesova 11, 041 54 Košice, Slovak Republic*
[c]*Department of Food Hygiene, Technology and Safety, University of Veterinary Medicine and Pharmacy, Komenského 73, 041 81 Košice, Slovak Republic*
[d]*Department of Inorganic Chemistry, Faculty of Science, Charles University, Hlavova 2030, 128 00 Prague, Czech Republic*
[e]*Department of Pharmaceutical Technology, Pharmacognosy and Botany, University of Veterinary Medicine and Pharmacy, Komenského 73, 041 81 Košice, Slovak Republic*
[f]*NMR laboratory, Faculty of Science, P.J.Šafárik University, Moyzesova 11, 041 54 Košice, Slovak Republic*
[g]*Department of Pharmacology, Faculty of Medicine, P.J.Šafárik University, Trieda SNP 1, 040 11 Košice, Slovak Republic*
[h]*Department of Molecular Electrochemistry and Catalysis, J. Heyrovský Institute of Physical Chemistry of the CAS, Dolejškova 3/2155, 182 23 Praha 8, Czech Republic*

†Electronic supplementary information (ESI) available. CCDC 2331721 and 2331722. For ESI and crystallographic data in CIF or other electronic format see DOI: https://doi.org/10.1039/d4dt00389f



This journal is © The Royal Society of Chemistry 2024

Published on 12 April 2024. Downloaded on 3/12/2025 6:23:37 AM.

the treatment of cancer and infectious diseases. However, the side effects as well as the resistance of commercially used drugs lead to the search for new approaches to the treatment of the mentioned diseases. One approach is to support the naturally occurring mechanisms of the individual's immune system. In recent decades, new drugs based on antimicrobial peptides (AMPs) (their natural production is one of the immune responses of organisms to pathogens) have been intensively studied against highly resistant pathogenic microorganisms, while last year their latest classification was presented in terms of structure, mechanism of action, as well as preparation methods.[1] In addition, it was found that many investigated AMPs also have anticancer activity.[2–5] However, a large amount of published knowledge (mainly about their specific effect against cancer) has led to comprehensive articles focusing on a separate group of potential drugs, namely anticancer peptides (ACPs). Although about 1500 review articles have been published about this group of peptides (according to WOS),[6] the article by Campos *et al.* from 2023[7] offers an interesting bibliometric analysis of anticancer peptides in terms of their composition, structure, and effect. Similarly to AMPs, the amino acid composition of the ACPs is of the utmost importance since they may determine the function they exert. For example, the presence of proline and glycine, aliphatic nonpolar amino acids in anticancer peptides, appears crucial for membrane interaction and conformational flexibility.[7]

Proline and its derivative hydroxyproline, as a part of AMPs and ACPs, are non-essential amino acids in humans synthesized either by several-step biosynthesis (proline) or by hydroxylation of the amino acid proline by the enzyme prolyl hydroxylase following protein synthesis (as a post-translational modification, hydroxyproline).[8,9] Proline and hydroxyproline ensure many bioprocesses that Minchiotti *et al.* summarized[10] in a review article, which shows that proline metabolism influences beneficial tissue regeneration, but also contributes to the progression of devastating pathologies such as fibrosis and metastatic cancer.

Since proline and its derivatives are part of many biological processes, in addition to commercially used proline-based drugs in the treatment of high blood pressure (angiotensin-converting enzyme (ACE) inhibitors, fosinopril, enalapril, captopril, *etc.*), proline-based antimicrobial and anticancer peptides are also being isolated as potential and promising drugs.[10–14]

New metal–peptide complexes are increasingly being prepared and investigated as potential drugs due to the interesting and specific properties of metal ions.[15] Proline derivatives provide an interesting ligand environment for antimicrobial and anticancer active metal ions such as Ru, Pd, Pt, Au, Cu and Sn, and in the case of these complexes the $IC_{50}$ values against selected cancer cell lines are in micromolar concentrations (in the order of units to hundreds).[16–20] The most prepared crystalline complexes of proline and hydroxyproline were with the biologically active central atoms Cu (43) and Pd (37), and then Ru (22), Zn (16), Pt (15), and Ag(2).[21,22–26] Only in the case of Pt(II) complexes (K[$PtCl_2$(L-Pro)] and [PtCl(DMSO)(L-Pro)]) was cytotoxic activity observed against four selected human cancer cell lines (anaplastic thyroid cancer 8505C, head and neck cancer A253, lung cancer A549, and colon cancer DLD-1 cells).[27]

Therefore, as part of our long-term work devoted to the preparation of complexes with naturally occurring ligands in organisms that are part of the immune system (*e.g.* amino acids and peptides), we present the isolation of silver(I) complexes with Pro and Hyp. For their possible use in the treatment of infections or cancer, we performed their full characterization in the solid phase and also observed their stability in the test solution used as a stock solution during antibacterial and anticancer studies. In the case of *in vitro* antibacterial studies, we used two fundamentally different methods to point out caution when correlating the results obtained by different methods. Moreover, we determined their anticancer activity *in vitro* and tried to outline the mechanism of their behaviour in the presence of the most abundant protein in the blood to predict their pharmacokinetics. In addition, the potential of the new complexes to irritate vessels and their bioavailability (experimental and theoretical correlations) were evaluated and discussed.

## Results and discussion

### Syntheses of complexes

Although the preparation of the complexes $\{[Ag_2(Pro)_2(NO_3)]NO_3\}_n$ (AgPro) and $\{[Ag_2(Hyp)_2(NO_3)]NO_3\}_n$ (AgHyp) appears simple, their isolation required suitable conditions for the formation of single crystals appropriate for X-ray analysis. From our many attempts follows the fact that the crucial role is the correct setting of the reactant amounts to the reaction medium (whether an aqueous or aqueous-ethanolic) amount. In contrast, a reactant ratio changing (from 1 : 1 to 1 : 2, Ag : ligand) led to the formation of single crystals with the same composition. The final compounds are stable in air and their solubility at 0.5 mg $mL^{-1}$ was studied in different solvents. Complex AgPro was found to be very soluble in deionized water, DMSO and DMF, slightly soluble in ethanol and methanol at 60 °C and insoluble in acetone and THF. AgHyp is similarly very soluble in deionized water, but slightly soluble in DMSO, methanol and THF at 60 °C and insoluble in ethanol, acetone and DMF. Due to their possible sensitivity to light, the complexes are stored in the absence of light.

### Description of crystal structures

Complex AgPro crystallizes in the monoclinic lattice with space group $P2_1$. The asymmetric unit of the complex consists of two silver(I) ions, two molecules of Pro as zwitterions, and one coordinated and one uncoordinated nitrate anion. The crystal structure of coordination compound AgPro is depicted in Fig. 1a. Crystal data and structure refinement details are summarized in Table S1 in the ESI.†

Published on 12 April 2024. Downloaded on 3/12/2025 6:23:37 AM.

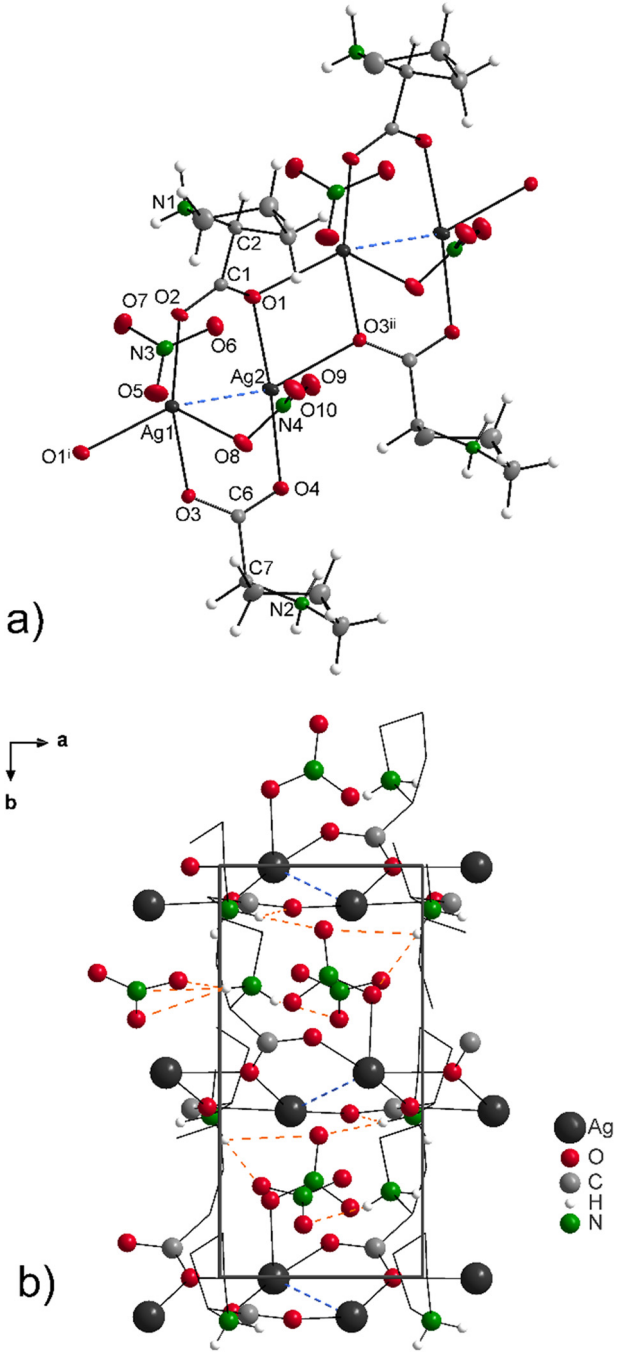


**Fig. 1** Crystal structure and atomic labelling scheme (i = $x + 1, y, z$; ii = $x - 1, y, z$) with ellipsoids drawn at the 50% probability level (a) and solid-state packing viewed along [001] (b) for AgPro with argentophilic interactions (blue dashed lines) and the hydrogen bond system (orange dashed lines).

The geometry identification of tetracoordinated metal ions is sometimes difficult especially when the structure is an intermediate between the two most common four-coordinate geometries, tetrahedral and square-planar.[28] Yang *et al.* proposed the formula for calculating the structural parameter $\tau_4 = (360 - (\alpha + \beta)/141) \times 100$, where $\alpha$ and $\beta$ are the two largest angles in a tetracoordinated complex. The value of $\tau_4$ = 0% is typical of the ideal square planar geometry ($D_{4h}$) while $\tau_4$ = 100% is typical of the ideal tetrahedral geometry ($T_d$). The value of $\tau_4$ in the range 0 to 100% corresponds to trigonal pyramidal and seesaw intermediate structures. The calculated values of $\tau_4$ for the Ag1 ion without consideration of Ag···Ag interactions is 58%, which indicates a distorted seesaw ($C_{2v}$) geometry. A similar distorted seesaw geometry around the silver(I) ion was also observed in the hydroxyprolinate complex $\{[Ag_2(HSSA)(Hyp)]_2{\cdot}3H_2O\}_n$ ($HSSA^{3-}$ = 5-sulfosalicylic acid)[29] with a reported parameter of $\tau_4$ = 66%. The second silver(I) ion Ag2 is coordinated by three oxygen atoms O1, $O3^{ii}$ (ii = $x - 1, y, z$) and O4, also from three Pro molecules.

The organic ligand adopts a *syn–syn–anti* bidentate-bridging coordination mode to silver(I) ions through carboxylate groups resulting in a 1D chain parallel with the *a* axis (Fig. 1a). The bond distances between the silver(I) ions and the *syn*-coordinated oxygen atoms from the carboxylate groups are in the range of 2.2210(18)–2.3605(17) Å. Similar bond distances were also observed in the complex $[CdCl_2(C_5H_9NO_2)]{\cdot}H_2O$[30] with a *syn–syn* bidentate bridging coordination mode of the prolinato ligand. The largest angle values in the complex AgPro are 165.63(7)° (for O2–Ag1–O3) and 152.80(8)° (for O4–Ag2–O1). The Ag–O bond distances between the silver(I) ions and *anti*-coordinated oxygen atoms are slightly longer (2.3887(17) and 2.4230(15) Å).

The carboxylate coordination mode and Ag–O bond distances are in good agreement with other published silver(I) amino acid complexes with the structural formulae $\infty\{[Ag(Hacgly)]_2\}$ (Hacgly = *N*-acetylglycine), $\{[Ag_2(D\text{-}Hasp)(L\text{-}Hasp)]{\cdot}1.5H_2O\}_n$ (Hasp = aspartic acid), $[Ag_2(HGly)_2]_n(NO_3)_{2n}$ (HGly = glycine), $\{[Ag_4(L\text{-}HAla)_4(NO_3)_3]NO_3\}_n$ (L-HAla = L-alanine) and $\{[Ag(HVal)(H_2O)(NO_3)]\}_n$ (HVal = valine) described in the literature.[31–35] Detailed bond lengths and angles are listed in Table S2 in the ESI.†

The coordination mode of the Pro molecules led to the formation of a 1D polymeric chain propagating along the *a* crystallographic axis with significant Ag–Ag interactions of 2.8375(3) Å (Fig. 1, blue dashed bonds). These contacts are shorter than the sum of their van der Waals radii (3.44 Å), indicating the presence of significant argentophilic interactions.[36]

In the neutral crystal form of AgPro the nitrate anions perform as counterions to the Ag(I) ions. The nitrato ligand including N4 is coordinated to a silver(I) ion by one oxygen atom O8 in monodentate coordination mode with a bond length of 2.592(2) Å. The same coordination mode of nitrato anion to silver(I) ions was also reported in other silver(I) complexes with the structural formulae $[Ag(dcypm)]_2(NO_3)_2$ (dcypm = bis(dicyclohexylphosphino)methane) and $\{[Ag_4(L\text{-}HAla)_4(NO_3)_3]NO_3\}_n$, with Ag–O($NO_2$) bond distances 2.557(9)[37] and 2.557(2) Å.[34] The second nitrate anion (N3) is in ionic form, which is caused by the long distance between the silver(I) ion and oxygen atom (2.7177(22) Å).

The 3D crystal structure is stabilized by N–H···N and N–H···O intermolecular hydrogen bonding interactions (Fig. 1b, orange dashed bonds; see Table S3†).


This journal is © The Royal Society of Chemistry 2024

Published on 12 April 2024. Downloaded on 3/12/2025 6:23:37 AM.

Similar to the AgPro complex, the coordination compound AgHyp crystallizes in the monoclinic lattice with space group $P2_1$. Moreover, the structural properties, such as the composition of the asymmetric unit, the geometries around the silver (I) ions and the coordination modes of the ligand Hyp and the nitrate anion, are the same as in the case of complex AgPro. The crystal structure of complex AgHyp is depicted in Fig. 2a. Crystal data and structure refinement details are summarized in Table S1 in the ESI.†

The calculated value of $\tau_4$ for the Ag2 ion without consideration of Ag···Ag interaction is 51%, which also indicates a distorted seesaw ($C_{2v}$) geometry. The bond distances between the silver(I) ions and coordinated oxygen atoms from the carboxylate groups are in the range of 2.184(6)–2.522(8) Å (Table S4†). These bond distances are in great accordance with another silver(I) hydroxyprolinate complex $\{[Ag_2(HSSA)(Hypo)]_2{\cdot}3H_2O\}_n$ (Hypo = (2*S*,4*R*)-4-hydroxyproline; $HSSA^{3-}$ = 5-sulfosalicylic acid) determined by Zorlu *et al.*[29] Moreover, the same bidentate bridging coordination mode was observed in the case of this complex. Similarly, the coordination mode of the Hyp molecules led to the formation of a 1D polymeric chain propagating along the *a* crystallographic axis with significant argentophilic interactions of 2.8756(9) Å (Fig. 2a, blue dashed bonds).[36] The Ag–O bond distance between the silver(I) ion and the coordinated oxygen atom of the nitrate anion (N3) is 2.5947(74) Å. The 3D crystal structure is stabilized by N–H···N, O–H···O and N–H···O intermolecular hydrogen bonding interactions (Fig. 2b, orange dashed bonds). Detailed hydrogen bond interactions are summarized in Table S5.†

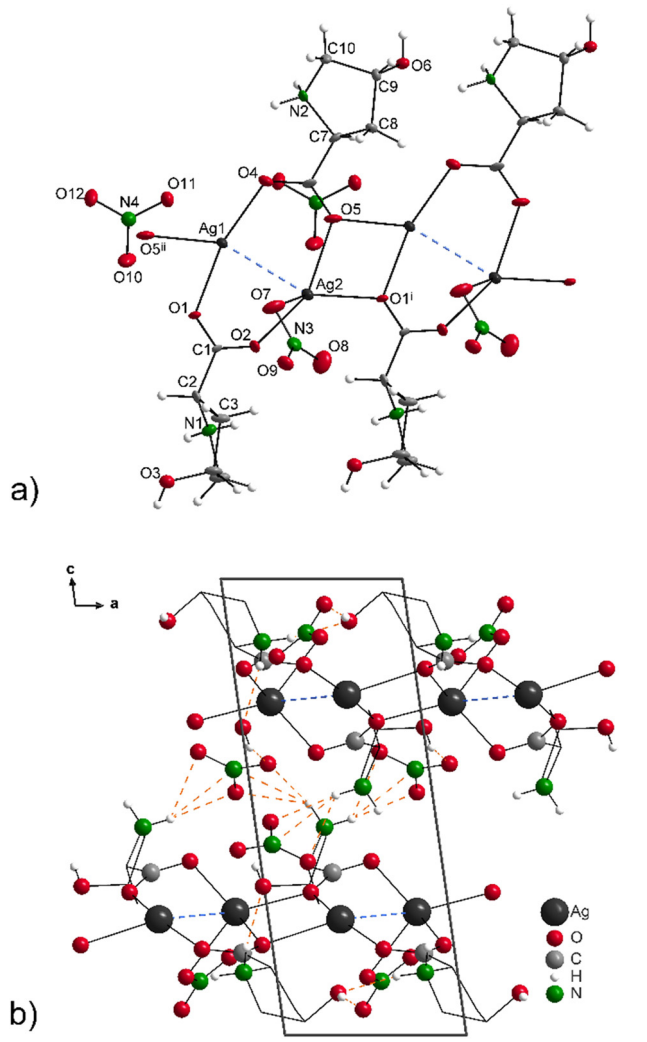


**Fig. 2** Crystal structure and atomic labelling scheme (i = *x* + 1, *y*,*z*; ii = *x* − 1, *y*,*z*) with ellipsoids drawn at the 50% probability level (a) and solid-state packing viewed along [010] (b) for AgHyp with argentophilic interactions (blue dashed lines) and the hydrogen bond system (orange dashed lines).

## Infrared spectra

The FT-IR spectra of ligands Pro, Hyp and their appropriate silver(I) complexes are depicted in Fig. S1.† Characteristic vibration bands are noted in Table S6.†

Based on the literature,[38] in the spectra of ligand Hyp and AgHyp the bands at 3270 and 3261 $cm^{-1}$ are assigned to the OH stretching vibration. The vibration bands observed in the region of 3330–2820 $cm^{-1}$ for both free ligands and silver(I) complexes belong to $NH_2^+$ and $CH_2$ stretching vibrations. The scissoring vibrations of the $CH_2$ group were observed only in the spectra of Pro and AgPro at 1472 and 1471 $cm^{-1}$, respectively. In all recorded spectra the wagging vibration ($\omega$) of the mentioned functional group appears at lower wavenumber values, in the range from 1335 to 1375 $cm^{-1}$. This observation is in great correlation with the literature.[38–40] The differences in the wavenumber values between the carboxylate asymmetric and symmetric stretching vibrations of the ligands depicted in Fig. S1 and Table S6† confirm their coordination to the silver (I) ions. Moreover, the absence of a strong vibration band at 1700 $cm^{-1}$ clearly indicates the presence of the $COO^-$ function in zwitterionic form.[38] The asymmetric stretching vibration changes the wavenumber from lower, 1552 (for Pro), to higher, 1561 $cm^{-1}$ (for AgPro), and from higher, 1574 (for Hyp), to lower, 1569 $cm^{-1}$ (for AgHyp), values. The opposite trend was observed in the case of carboxylate symmetric stretching vibrations (see Table S6†). These vibrations are also sensitive to the metal ion coordination mode.[35,41] Wavenumber differences $\Delta(\nu_{as} - \nu_s)$ indicate bidentate bridging carboxylate coordination modes for the complexes AgPro ($\Delta$ = 143 $cm^{-1}$) and AgHyp ($\Delta$ = 156 $cm^{-1}$). This coordination mode was confirmed by X-ray analysis. A similar band shifting was observed in the spectra of the $[MnCl_2(C_5H_9NO_2)]{\cdot}H_2O$ and $\{[Ag_2(HSSA)(Hypo)]_2{\cdot}3H_2O\}_n$ (Hypo = (2*S*,4*R*)-4-hydroxyproline; $HSSA^{3-}$ = 5-sulfosalicylic acid) complexes mentioned in Rzączyńska[42] and Zorlu *et al.*[29] with $\Delta$ values 170 and 142 $cm^{-1}$, respectively. The small wavenumber differences ($\Delta\nu_3$ = 90 $cm^{-1}$ (for AgPro), $\Delta\nu_3$ = 79 $cm^{-1}$ (for AgHyp); and $\Delta\nu_4$ = 13 $cm^{-1}$ (for AgPro), $\Delta\nu_4$ = 33 $cm^{-1}$ (for AgHyp) (Table S6†)) between the vibration bands corresponding to asymmetric stretch ($\nu_3$) and in-plane bending ($\nu_4$) vibrations of the nitrate anions indicate the monodentate coordination of the nitrate anions to silver(I) ions in both silver(I) complexes. This coordination mode was

Published on 12 April 2024. Downloaded on 3/12/2025 6:23:37 AM.

also confirmed by X-ray analysis. Moreover, the vibration band at 1288 $cm^{-1}$ for AgPro and 1318 $cm^{-1}$ for AgHyp indicates the presence of free $NO_3^-$ anions. A similar trend was observed in the case of two Cu(II) complexes based on bitopic bis(pyrazol-1-yl)methane ligands.[43] In all the spectra the pyrrolidine ring stretching mode appears at around 1030 and 920 $cm^{-1}$. The bending mode is observed in the lower range of wavenumbers from 603 to 693 $cm^{-1}$. The other characteristic vibration bands have been identified and their assignments are listed in Table S6.†

### Thermogravimetric analysis

The TG curves of bitopic AgPro and AgHyp complexes are shown in Fig. S2.† Complex AgPro is thermally stable to 170 °C, while the thermal stability of complex AgHyp is slightly lower (155 °C). The thermal decompositions of the inorganic–organic parts (Pro/Hyp and $NO_3^-$ anions) are observed in the range 170–450 and 156–400 °C, with an experimental weight loss of 63.08% (calcd 62.15%) for complex AgPro and 64.17% (calcd 64.16%) for complex AgHyp. The final decomposition product is elemental silver (exp. 36.92%, calcd 37.85% (AgPro); exp. 35.83%, calcd 35.84% (AgHyp)). A higher thermal stability (218 °C and 240 °C) was observed in the case of the cadmium (II) complexes, $[Cd(L\text{-Pro})_2Br_2]$[44] and $[Cd(L\text{-Hyp})Br_2]$,[45] respectively.

### Complexes' stability in solution

**NMR spectra.** To confirm the composition and stability of the AgPro and AgHyp complexes in the biological test medium DMSO, we compared the changes in the spectra of the free ligands and their silver(I) complexes. The complexes were fully characterized, and their $^1H$ and $^{13}C$ NMR (Fig. 3, and Fig. S3†) assignments were unambiguously determined using splitting patterns, chemical shifts, and 2D NMR data from COSY, NOESY (Fig. 4, and Fig. S4†), HSQC, and HMBC (Fig. 5, and Fig. S5†) spectra. The $^1H$ and $^{13}C$ NMR data of complexes AgPro and AgHyp are summarized in Tables 1 and 2. In the $^1H$ NMR spectra, sharp, well-resolved signals implied a stable and unchanging coordination of L-proline or *trans*-4-hydroxy-L-proline donor atoms to the silver(I) centre at 298 K.

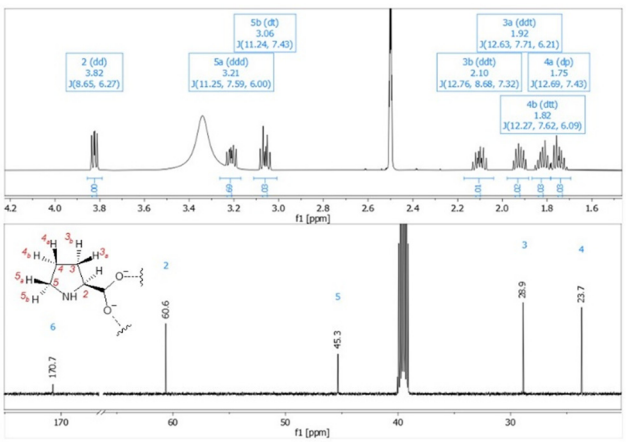


**Fig. 3** $^1H$ NMR (600 MHz, DMSO-$d_6$) and $^{13}C$ NMR (150 MHz, DMSO-$d_6$) spectra of complex AgPro.

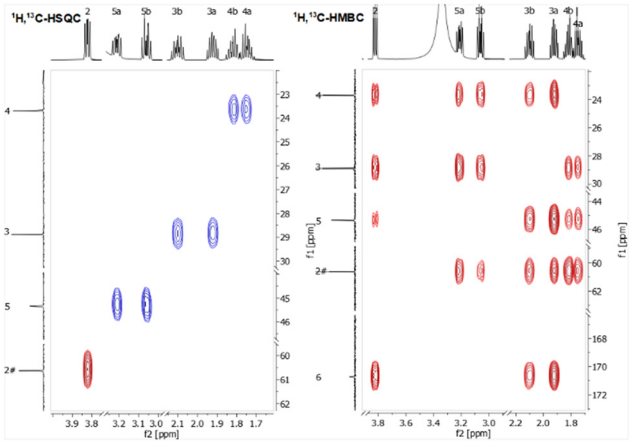


**Fig. 4** $^1H,^1H$-COSY and $^1H,^1H$-NOESY (DMSO-$d_6$) spectra of complex AgPro.

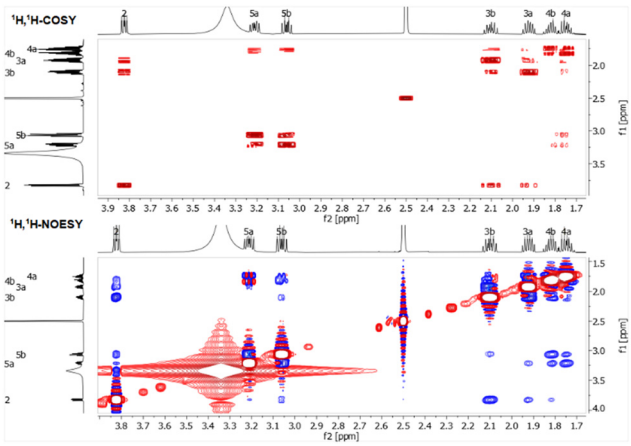


**Fig. 5** $^1H,^{13}C$-HSQC and $^1H,^{13}C$-HMBC (DMSO-$d_6$) spectra of complex AgPro.

Regarding the structure of complex AgPro, the $^1H,^1H$-COSY spectrum (Fig. 4) revealed cross-peaks between 3.82 ppm (dd, $J$ = 8.7, 6.2 Hz) and 2.10 ppm (ddt, $J$ = 12.8, 8.7, 7.3 Hz) and 1.92 ppm (ddt, $J$ = 12.6, 7.7, 6.2 Hz), which correlated with $^{13}C$ NMR signals at 60.6 and 28.9 ppm, respectively, in the HSQC spectrum (Fig. 5). Consequently, these shifts were assigned to H2/C2 and H3a/C3 and H3b/C3, with the coupling constant $J$ = 8.7 Hz between H2 and H3b indicating their *cis* position and the coupling constant $J$ = 6.2 Hz between H2 and H3a indicating their *trans* position. Assignments for H4 and H5 protons were made based on COSY and NOESY correlations (Fig. 4). In the NOESY spectrum, proton H2 correlated with the proton H4b signal at 1.82 ppm (dtt, $J$ = 12.3, 7.6, 6.1 Hz), and the signal at 1.75 ppm (dp, $J$ = 12.7, 7.4 Hz) was identified as proton H4a. Protons H4a and H4b showed HSQC correlations with carbon at 23.7 ppm. Furthermore, H4b showed a NOESY


This journal is © The Royal Society of Chemistry 2024

Published on 12 April 2024. Downloaded on 3/12/2025 6:23:37 AM.

**Table 1** $^{1}$H NMR (600 MHz, DMSO-$d_6$) chemical shifts ($\delta$, ppm) of AgPro and AgHyp complexes as well as the free ligands Pro and Hyp

| $\delta_H$ | H2↓ | H3a | H3b↓ | H4a | H4b↓ | H5a | H5b↓ | OH |
|---|---|---|---|---|---|---|---|---|
| Pro | 3.61 (dd, 8.7, 5.5) | 1.92 (ddt, 12.8, 7.3, 5.6) | 2.01 (dq, 12.8, 7.9) | 1.67 (dq, 12.6, 7.6) | 1.77 (dtt, 12.7, 7.3, 5.6) | 3.21 (ddd, 11.2, 7.6, 5.6) | 2.99 (dt, 11.2, 7.6) | — |
| AgPro | 3.82 (dd, 8.7, 6.2) | 1.92 (ddt, 12.6, 7.7, 6.2) | 2.10 (ddt, 12.8, 8.7, 7.3) | 1.75 (dp, 12.7, 7.4) | 1.82 (dtt, 12.3, 7.6, 6.1) | 3.21 (ddd, 11.3, 7.6, 6.0) | 3.06 (dt, 11.2, 7.4) | — |
| $\Delta$(AgPro–Pro) | 0.21 | 0 | 0.09 | 0.08 | 0.05 | 0 | 0.07 | — |
| Hyp | 3.75 (t, 8.8) | 1.85 (m) | 2.05 (m) | 4.30 (s) | — | 3.18 (dd, 12.1, 4.1) | 2.91 (d, 12.1) | 5.20 (s) |
| AgHyp | 3.97 (dd, 10.2, 7.6) | 1.90 (ddd, 13.8, 10.2, 4.5) | 2.12 (dd, 13.8, 7.7) | 4.34 (d, 4.7) | — | 3.25 (dd, 12.0, 4.2) | 2.97 (dt, 12.0, 1.8) | 5.31 (s) |
| $\Delta$(AgHyp–Hyp) | 0.22 | 0.05 | 0.07 | 0.04 | — | 0.07 | 0.06 | 0.11 |

**Table 2** $^{13}$C NMR (150 MHz, DMSO-$d_6$) chemical shifts ($\delta$, ppm) of the AgPro and AgHyp complexes as well as free ligands Pro and Hyp. *Hyp partly soluble in DMSO-d6, $m$ = 10 mg, impossible to measure the $^{13}$C NMR spectrum

| $\delta_C$ | $COO^-$ | C2 | C3 | C4 | C5 |
|---|---|---|---|---|---|
| Pro | 169.1 | 60.7 | 28.9 | 23.9 | 45.2 |
| AgPro | 170.7 | 60.6 | 28.9 | 23.7 | 45.3 |
| $\Delta$(AgPro–Pro) | 1.6 | −0.1 | 0 | −0.2 | 0.1 |
| Hyp* | nd | nd | nd | nd | nd |
| AgHyp | 170.0 | 59.5 | 38.1 | 69.3 | 53.0 |

correlation with proton H5b at 3.06 (dt, $J$ = 11.2, 7.4 Hz), and the proton signal at 3.21 ppm (ddd, $J$ = 11.3, 7.6, 6.0 Hz) was identified as proton H5a.

The coordination mode of the ligands Pro and Hyp was confirmed by comparing the $^{1}$H NMR spectral data of the ligand with the corresponding data in the complex. The binding of the silver(I) ion to the oxygen atoms of the carboxyl group induced a shift of protons H-2, H-3, H-4, and H-5 to higher $\delta_H$ values in the $^{1}$H NMR spectrum of the complex (Table 1). A significant downfield shift of the protons of the complex compared with the corresponding ligand confirmed the coordination of the carboxyl oxygens.

Surprisingly, the $^{13}$C NMR chemical shifts were only slightly affected by the coordination. It is noteworthy that the carboxyl carbon of AgPro shifted to a higher $\delta_C$ value from 169.1 ppm in the ligand spectrum to 170.7 ppm in the complex spectrum. Conversely, the signals of carbon atoms C-2 and C-4 slightly shifted to lower $\delta_C$ values (Table 2).

Moreover, the stability of the prepared compounds in DMSO solution was tested by $^{1}$H NMR measurements in a time scale of 96 h. Fig. S6† shows that the changes in chemical shifts in both time-dependent NMR spectra are not observed, and therefore the prepared silver(I) compounds were found to be stable in 1% DMSO-$d_6$/$D_2O$ solution for 96 h of biological testing.

The conductivity data for the complexes AgPro and AgHyp measured in DMSO indicate that these complexes behave as 1 : 1 electrolytes with $NO_3^-$ as counter-ion for a positively charged Ag(I) complex unit. A similar trend was observed in the case of $[Ag(CH_3CN)(py\text{-}2py)]BF_4$ complex with $BF_4^-$ as counter-ion for a positively charged complex unit.[46]

In addition, to estimate the biologically active species in DMSO, monomeric and dimeric structures of the complexes were optimized at three levels:

(a) xTB/GFN2, ALPB (dimethylsulfoxide);[47–52]

(b) B3LYP/3-21G, CPCM (dimethylsulfoxide);[53]

(c) M06-2X/6-311+G(d,p) basis set (for C, H, N, O, S atoms) and LANL2TZ(f) quasirelativistic effective-core potential, CPCM (dimethylsulfoxide).[53]

The identity of the minima was verified by the absence of imaginary vibrational frequencies. The equilibrium constants ($\log K$) as well as the corresponding changes in free energy $\Delta G_r^\circ$ (Table 3) were corrected (i) for the standard state volume (1 M, for Gaussian 16 results only) and (ii) for the solvent concentration (DMSO, $c$ = 14.1 mol dm$^{-3}$, $a$ = 1); *i.e.* the reported data are related to thermodynamic standard state.

Comparing the achieved equilibrium data for the monomeric and dimeric structures we concluded the presence of dimeric complex species in DMSO (according to the X-ray-determined structures Fig. 1a and 2a, see Table 3).

## Antibacterial activity

To determine the antibacterial activity, we have selected representative bacterial strains that cause milder but also very serious infection diseases. The antibacterial activity of the AgPro and AgHyp complexes and AgSD (the commonly used antibacterial active ingredient with silver(I) composition) was observed by two antibacterial activity tests, disk diffusion and microdilution. In both cases the same bacterial suspensions were used. Surprisingly, using the disk diffusion method, no antibacterial activity was confirmed against all the selected resistant bacteria even at the highest used concentration of the complexes of 0.5 mM (an inhibition zone was not observed). In contrast, using a microdilution approach for *Pseudomonas aeruginosa*, the MIC for AgPro and AgHyp was 0.063 mM and for *Staphylococcus aureus* was 0.063 mM (AgPro) and 0.016 mM (AgHyp), respectively (Table 4). Inhibition of *Bacillus cereus* growth was observed at 0.031 (AgPro) and 0.063 mM (AgHyp) concentrations of the newly synthesized compounds. The measured absorbance at 600 nm for complexes AgPro and

Published on 12 April 2024. Downloaded on 3/12/2025 6:23:37 AM.

**Table 3** Gibbs free energy changes ($T$ = 298.15 K, kJ mol$^{-1}$) and equilibrium constants of the estimated silver(I) complex species in DMSO biologically testing media optimized by three levels: (a) xTB/GFN2; (b) B3LYP/3-21G; (c) M06-2X/6-311+G(d,p) basis set (for C, H, N, O, S atoms) and LANL2TZ(f) quasirelativistic effective-core potential

| | $\log K$ | | | $\Delta G_r^\circ$ | | |
|---|---|---|---|---|---|---|
| Equilibrium | (a) | (b) | (c) | (a) | (b) | (c) |
| $2\ AgNO_3 + 2\ Pro = Ag_2Pro_2(NO_3)_2$ | 50.5 | 63.6 | 14.5 | −288.3 | −363.2 | −82.7 |
| $2\ AgNO_3 + 2\ Pro = Ag_2Pro_2NO_3^+ + NO_3^-$ | 47.3 | 38.6 | 13.0 | −270.1 | −220.1 | −74.1 |
| $2\ AgNO_3 + 2\ Pro = Ag_2Pro_2^{2+} + 2\ NO_3^-$ | 28.2 | 9.4 | 10.9 | −160.8 | −53.7 | −62.4 |
| $2\ AgNO_3 + 2\ Hyp = Ag_2Hyp_2(NO_3)_2$ | 48.1 | 64.6 | 15.3 | −274.5 | −369.0 | −87.5 |
| $2\ AgNO_3 + 2\ Hyp = Ag_2Hyp_2NO_3^+ + NO_3^-$ | 46.5 | 39.0 | 12.0 | −265.4 | −222.7 | −68.6 |
| $2\ AgNO_3 + 2\ Hyp = Ag_2Hyp_2^{2+} + 2\ NO_3^-$ | 28.4 | 9.0 | 10.4 | −162.0 | −51.4 | −59.1 |
| $Ag_2Pro_2(NO_3)_2 + 4\ DMSO = 2\ Ag(DMSO)_2^+ + 2\ Pro + 2\ NO_3^-$ | −18.8 | −43.4 | −5.0 | 107.2 | 247.5 | 28.6 |
| $Ag_2Hyp_2(NO_3)_2 + 4\ DMSO = 2\ Ag(DMSO)_2^+ + 2\ Hyp + 2\ NO_3^-$ | −16.4 | −44.4 | −5.8 | 93.4 | 253.3 | 33.4 |
| $Ag_2Pro_2NO_3^+ + 4\ DMSO = 2\ Ag(DMSO)_2^+ + 2\ Pro + NO_3^-$ | −15.6 | −18.3 | −3.5 | 89.0 | 104.4 | 20.0 |
| $Ag_2Hyp_2NO_3^+ + 4\ DMSO = 2\ Ag(DMSO)_2^+ + 2\ Hyp + NO_3^-$ | −14.8 | −18.7 | −2.5 | 84.3 | 107.0 | 14.5 |
| $Ag_2Pro_2^{2+} + 4\ DMSO = 2\ Ag(DMSO)_2^+ + 2\ Pro$ | 3.6 | 10.9 | −1.5 | −20.4 | −62.0 | 8.3 |
| $Ag_2Hyp_2^{2+} + 4\ DMSO = 2\ Ag(DMSO)_2^+ + 2\ Hyp$ | 3.3 | 11.3 | −0.9 | −19.1 | −64.4 | 5.0 |

**Table 4** Minimum inhibitory concentrations (MIC, mM) of complexes AgPro and AgHyp, ligands Pro and Hyp and standards $AgNO_3$ and AgSD on the tested bacteria

| | *Bacillus cereus* MIC [mM] | *Pseudomonas aeruginosa* MIC [mM] | *Staphylococcus aureus* MIC [mM] |
|---|---|---|---|
| AgPro | 0.031 | 0.063 | 0.063 |
| AgHyp | 0.063 | 0.063 | 0.016 |
| Pro | 0.5 | 0.5 | 0.125 |
| Hyp | 0.250 | 0.250 | 0.5 |
| $AgNO_3$ | 0.063 | 0.063 | 0.063 |
| AgSD | 0.031 | >0.5 | 0.016 |

AgHyp at a concentration range from 0.5 to 0.008 mM in the presence of the tested bacteria is in Table S7.†

Comparing the effect of free silver(I) ions (in the form of $AgNO_3$) and the new complexes (using a broth microdilution assay), it is clear that the silver(I) ion coordination by the Pro and Hyp ligands leads to its antibacterial effect increase against *Staphylococcus aureus* (AgHyp) and *Bacillus cereus* (AgPro) while free ligand antibacterial activity testing (Pro and Hyp) points out only their slight inhibitory effect on bacterial growth (Table 4). It follows from the above that both complexes provide a synergistic effect against *Bacillus cereus* (AgPro) and *Staphylococcus aureus* (AgHyp). In addition, both complexes are significantly more effective against *Pseudomonas aeruginosa* (a Gram-negative bacterium with low sensitivity to antibiotics) than commercially used AgSD.

As we presented in our previous work,[54] within the discussion of the achieved results, it is necessary to pay attention to the same experimental conditions. A similar approach, a comparison of the antibacterial activity of local antimicrobial agents against multidrug-resistant bacteria recovered from burn patients by two methods (disk diffusion and microdilution) was presented by Murray *et al.*[55] They also reported that some antibiotics (in the form of solutions of pure active substances) were not effective by the microdilution method, but in contrast were effective in a disk diffusion analysis (in the form of creams).

Comparing the abovementioned with our results, it can be concluded that using the agar disk diffusion method, we did not observe an inhibition zone caused by our tested compounds. However, it is important to mention that the choice of medium also influences the inhibition zone diameters as recorded by Brenner *et al.*[56] On the other hand, by the microdilution method, important MICs were observed for both complexes against selected bacterial strains and they even appear better than for the silver(I)-amino acid complexes determined by Nomiya[32] and topical antimicrobials containing silver(I) nitrate and silver(I) sulfadiazine tested by Murray (in the case of *Pseudomonas aeruginosa*). However, as we mentioned earlier, the comparison is not reliable because modified experimental conditions were used.

## Cytotoxic activity

An MTS colorimetric metabolic assay was used to evaluate the potential growth inhibitory effect of silver(I) complexes with amino acids (AgPro and AgHyp) on a panel of cancer cell lines with different origins and the most serious and frequently occurring forms of cancer (Table 5). The results were compared with human dermal fibroblasts as a model of normal cells and with cisplatin as a cytostatic agent used in cancer therapy. As the results showed, AgPro complex compared with AgHyp was more effective in inhibiting cancer cell metabolism in HCT116, MDA-MB-231, A2058, PaTu8902, HepG2 and Jurkat cancer cell lines. In the case of the HCT116, A2058, PaTu8902 cancer cell lines, the effect is even higher, but non-selective.

In contrast, the complexes' activity against MDA-MB-231 and Jurkat cancer cell lines is more than 7× higher for AgPro and more than 3× higher for AgHyp (in the case of MDA-MB-231) and 2× higher for AgPro and almost the same for AgHyp (in the case of Jurkat) compared with cisPt. Moreover, both AgPro and AgHyp show higher selectivity than

 This journal is © The Royal Society of Chemistry 2024

Published on 12 April 2024. Downloaded on 3/12/2025 6:23:37 AM.

**Table 5** Cytotoxic activity of silver(I) complexes AgPro and AgHyp, amino acids Pro and Hyp and cisPt against selected cancer lines and fibroblasts characterized by the predictive $IC_{50}$ (μM)

| | HeLa | HCT116 | MDA-MB-231 | A549 | A2058 | PaTu8902 | HepG2 | Jurkat | BJ-5ta |
|---|---|---|---|---|---|---|---|---|---|
| AgPro | 40.0 ± 0.0 | 9.3 ± 3.7 | 3.7 ± 0.1 | 16.1 ± 1.4 | 11.4 ± 2.2 | 19.6 ± 1.9 | 15.4 ± 0.5 | 3.0 ± 0.1 | 11.3 ± 1.8 |
| AgHyp | 32.2 ± 0.1 | 15.4 ± 4.0 | 7.7 ± 0.1 | 16.1 ± 2.3 | 21.5 ± 5.5 | 32.5 ± 0.3 | 17.5 ± 4.8 | 6.0 ± 0.1 | 12.3 ± 2.1 |
| Pro | >100 | >100 | >100 | >100 | >100 | >100 | >100 | >100 | >100 |
| Hyp | >100 | >100 | >200 | >200 | >200 | >100 | >100 | >100 | >100 |
| $AgNO_3$ | 20.2 ± 2.3 | 5.6 ± 1.4 | 6.1 ± 0.3 | 7.8 ± 1.8 | 7.4 ± 1.3 | 6.5 ± 0.6 | 5.5 ± 0.1 | 5.7 ± 0.0 | 10.5 ± 2.1 |
| cisPt | 30.4 ± 1.4 | 14.5 ± 2.5 | 26.7 ± 5.0 | 17.3 ± 2.2 | 18.8 ± 5.5 | 20.7 ± 3.1 | 14.0 ± 2.8 | 6.2 ± 0.1 | 31.0 ± 0.7 |

HeLa – human cervical adenocarcinoma, HCT116 – human colorectal carcinoma, MDA-MB-231 – human mammary gland adenocarcinoma, A549 – human alveolar adenocarcinoma, A2058 – human melanoma, PaTu8902 – human pancreatic adenocarcinoma, HepG2 – human hepatocellular carcinoma, Jurkat – human leukemic T cell lymphoma, BJ-5ta – human fibroblasts.

cisPt against MDA-MB-231 cancer cell lines (SI = 3.05 (AgPro); 1.60 (AgHyp); 1.16 (cisPt)). At the same time, comparing the $IC_{50}$ values of the $AgNO_3$ salt, cisPt and our complexes, it can be concluded that the anticancer effect of free silver(I) ions is the highest for all the monitored cancer cell lines except MDA-MB-231 and Jurkat, where the effect of AgPro is approximately 2× higher, which points to the fact that silver(I) in the form of the AgPro complex can be more accessible to rapidly proliferating breast cancer tissue with a high proline content and thus potentially effective during proline catabolism in regulating the growth and survival of cancer cells.[57]

### Determination of safety application

The Hen's Egg test or Hühner–Embryonen–Test (HET) is an *in ovo* method for investigation of the vasoirritation potential of different substances on the chorioallantoic membrane (CAM) of chicken embryos.[58] CAM is a highly vascularized embryonic membrane, which responds similarly to vaginal, mucosal, or eye tissue.[59–61] The chemical irritation of new materials can be based on the nonphysiological pH, salt concentration, osmolarity, or toxicity to cells. Such an irritation effect after local application leads to undesirable pain, and an inflammatory process followed by tissue damage. *In ovo* tests represent a gap between *in vitro* and *in vivo* tests. However, sometimes they are defined as *in vivo* methods.[62]

The concentration 30 μM was selected according to previous results about proliferation. This concentration and also a lower concentration were active on different cancer cell lines (HCT116, MDA-MB-231, A549, A2058, HepG2, Jurkat). It is also ten times higher than the last active concentration (Jurkat, 3.0 μM). In general, higher concentrations are used for *in vivo* and *in ovo* methods compared with *in vitro* tests.

The HET test was used according to the ICCVAM – Recommended Test Methods (NIH Publication no. 10-7553-2010). In this test, the negative effect of substances administered on the chorioallantoic membrane is evaluated by time and calculated as an irritation score. Three parameters are determined: lysis of blood vessels, haemorrhage, and intravascular coagulation and/or extravascular coagulation. Neither of the two tested substances AgPro or AgHyp shows a negative effect on CAM (Fig. 6). Moreover, no vasodilatation or vasoconstriction was also detected. Negative control – phosphate buffer – shows no effect and positive controls (1% SDS and 1 M NaOH) show severe irritation. The results predicted that both substances are safe for different types of application. For example, they can be administered without any irritation to mucous membranes, such as vaginal,[63] nasal[64] or oral mucosae, so they can be used as part of dental products.[65] They can be also part of ocular products.[66] Except for local application, the HET assay shows the possibility for safe application in subcutaneous administration as was detected in the case of vaccine adjuvants.[64] The Hen's egg test on CAM substitutes the Draize rabbit eye irritancy assay,[67,68] so both substances should be used for ocular therapy without showing any irritation. This *in ovo* test predicted the safety of the topical and intravenous application of AgPro and AgHyp.

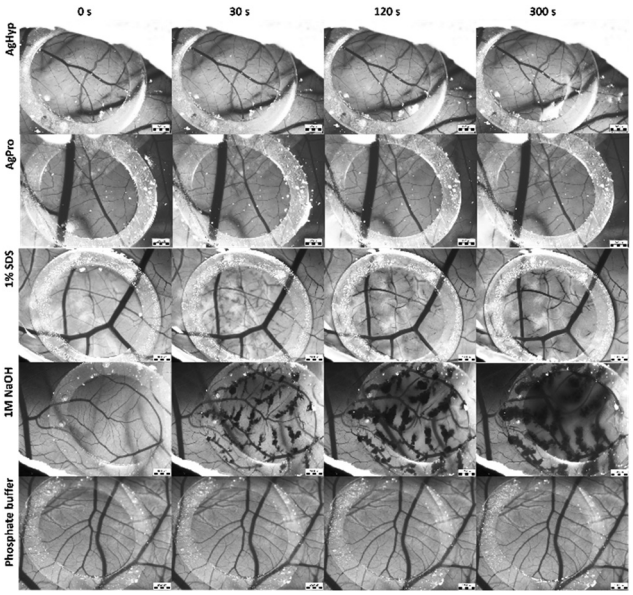


**Fig. 6** HET-CAM test of AgPro and AgHyp shows no irritation effects. Bar scale represents 1000 μm.

### Fluorescence quenching studies

The interactions of human or bovine serum albumin (HSA or BSA) with nano-complexes have obtained abundant interest in recent years due to their important impact in the field of

Published on 12 April 2024. Downloaded on 3/12/2025 6:23:37 AM.

medical therapy. The affinity of HSA (BSA) for various drugs affects their pharmacokinetics and efficacy. Although binding to HSA (BSA) helps to solubilize the drug in plasma, too strong an affinity limits the free/available forms of the drug, meaning that higher doses must be administered to achieve the desired drug efficacy *in vivo*.[69]

The interaction of BSA with silver(I) complexes was assessed by monitoring the intrinsic fluorescence intensity changes of BSA upon the addition of Ag(I) complexes at four temperatures (293.15 K, 298.15 K, 303.15 K and 308.15 K). The fluorescence quenching spectra of BSA without and with increasing concentrations of AgPro and AgHyp complexes at various temperatures are presented in Fig. 7 and 8 for 298.15 K and for 293.15, 303.15 and 308.15 K in the ESI (Fig. S7–S12†).

The results in Fig. 7 and 8 show that the fluorescence of BSA was intensely decreased by the addition of both complexes. From the classical Stern–Volmer equation (eqn (7), see Experimental section, inset Fig. 7 and 8) were calculated the Stern–Volmer constant ($K_{sv}$) for AgPro and AgHyp (Tables 6 and 7).

To determine the binding constant $K$, we used the modified Stern–Volmer eqn (1):

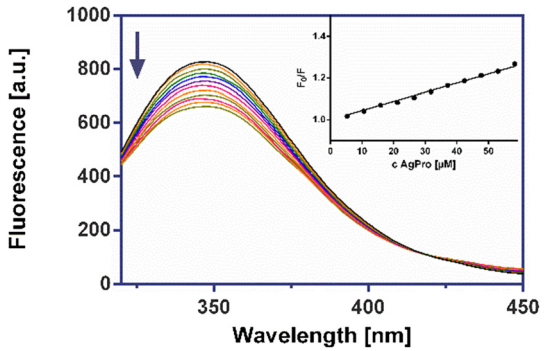


**Fig. 7** Fluorescence quenching spectra of BSA in the presence of AgPro. Inset: the corresponding Stern–Volmer plot for AgPro and BSA at 298.15 K.

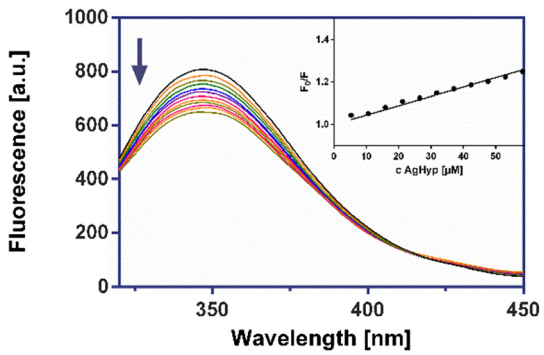


**Fig. 8** Fluorescence quenching spectra of BSA in the presence of AgHyp. Inset: the corresponding Stern–Volmer plot for AgHyp and BSA at 298.15 K.

**Table 6** Stern–Volmer values, binding constant and thermodynamic parameters of the interaction for the BSA–AgPro system at four different temperatures

| Temperature [K] | $K_{sv} \times 10^3$ [$M^{-1}$] | $K \times 10^4$ [$M^{-1}$] | $n$ | $\Delta G$ [kJ $mol^{-1}$] | $\Delta H$ [kJ $mol^{-1}$] | $\Delta S$ [J $mol^{-1}$ $K^{-1}$] |
|---|---|---|---|---|---|---|
| 293.15 | 4.35 ± 0.09 | 1.15 ± 0.12 | 1.10 | −15.38 | −14.70 | 52.40 |
| 298.15 | 4.16 ± 0.10 | 1.91 ± 0.20 | 1.15 | −15.64 | | |
| 303.15 | 3.73 ± 0.11 | 3.89 ± 0.27 | 1.22 | −15.90 | | |
| 308.15 | 3.36 ± 0.07 | 13.65 ± 0.43 | 1.34 | −16.16 | | |

**Table 7** Stern–Volmer values, binding constant and thermodynamic parameters of the interaction for the BSA–AgHyp system at four different temperatures

| Temperature [K] | $K_{sv} \times 10^3$ [$M^{-1}$] | $K \times 10^3$ [$M^{-1}$] | $n$ | $\Delta G$ [kJ $mol^{-1}$] | $\Delta H$ [kJ $mol^{-1}$] | $\Delta S$ [J $mol^{-1}$ $K^{-1}$] |
|---|---|---|---|---|---|---|
| 293.15 | 4.62 ± 0.10 | 2.63 ± 0.11 | 1.02 | −6.76 | −6.49 | 23.04 |
| 298.15 | 4.42 ± 0.06 | 3.24 ± 0.22 | 0.92 | −6.88 | | |
| 303.15 | 4.23 ± 0.04 | 4.68 ± 0.51 | 0.96 | −6.99 | | |
| 308.15 | 4.02 ± 0.03 | 7.76 ± 0.38 | 0.96 | −7.11 | | |

$$\log\left[\frac{(F_0 - F)}{F}\right] = \log K + n \log[Q] \quad (1)$$

where $K$ is the binding constant and $n$ is the number of binding sites and $F_0$ and $F$ are the fluorescence intensities in the absence and the presence of the silver complex. Hence the binding parameters, $K$ and $n$, can be obtained from the intercept and slope of the linear plot of $\log[(F_0 - F)/F]$ *versus* the log molar concentration [Q] of silver(I) complexes (Fig. S13(A), and S14(A)†).

The determined binding constant ($K$) and the number of binding sites ($n$) for the BSA–Ag(I) complex system are listed in Tables 6 and 7. The binding site value $n \approx 1$ may indicate the existence of only one binding site for AgPro and AgHyp complex in BSA.

The interaction between the quencher and BSA may be formed by hydrogen bonds, hydrophobic force, van der Waals interactions, electrostatic binding and others.[69] In order to map the interaction of Ag(I) complexes with BSA, the thermodynamic parameters were estimated using the Van 't Hoff equations, eqn (2) and (3).[70]

$$\log K = -\frac{\Delta H}{(2303RT)} + \frac{\Delta S}{2303R} \quad (2)$$

$$\Delta G = \Delta H - T\Delta S \quad (3)$$

The values of the entropy and enthalpy parameters identify the type of BSA–drug interactions. When $\Delta H < 0$ or $\Delta H \approx 0$ and $\Delta S > 0$, the main force is electrostatic in nature; when $\Delta H < 0$ and $\Delta S < 0$, the main force is due to hydrogen bonding or van der Waals interaction; and when $\Delta H > 0$ and $\Delta S > 0$, the main force is related to hydrophobic interactions.[71] The van 't Hoff plot for BSA–Ag(I) complexes is presented in Fig. S13(B) and S14(B).† The enthalpy change, the entropic change, and the free energy change were calculated from eqn (2) and (3). All parameters such as $\Delta S$, $\Delta G$, and $\Delta H$ for the interaction of


This journal is © The Royal Society of Chemistry 2024

Published on 12 April 2024. Downloaded on 3/12/2025 6:23:37 AM.

serum albumin with our silver(I) bioactive substances are summarized in Tables 6 and 7. The calculated binding constants ($K$) for AgPro are about 10 times higher than for AgHyp and the number of binding sites ($n$) on BSA for both complexes is approximately equal to one.

Fluorescence quenching can occur in a dynamic or static manner. In the case of dynamic fluorescence quenching the fluorophore in an excited state is deactivated upon collision with a quencher molecule and the dynamic quenching constants increase with increased temperatures. The static quenching is caused by the formation of a non-fluorescent complex in the ground state between the quencher and fluorophore. For the static quenching, the quenching constants reduce with the increase of temperature.[71]

Our fluorescence experiments demonstrated a static type of quenching mechanism because the values of $K_{sv}$ constant indicated a decreasing trend with rising temperature.[72]

The enthalpy and entropy values were $\Delta H < 0$ and $\Delta S > 0$, which indicates the presence of an electrostatic force of attraction. The negative value of $\Delta G$ suggests that AgPro and AgHyp bind to BSA spontaneously.[72]

### Zeta potential studies

Zeta potential (ZP, $\zeta$) can be used to monitor the surface charge properties of proteins. Changes in the ZP values can suggest conformational modifications, structure changes, surface, aggregation, unfolding or denaturation processes on the protein. Therefore, the ZP of BSA can be a technique for the determination of protein stability upon ligand binding.[73] Table 8 shows the zeta potential ($\zeta$) for BSA in the absence and in the presence of AgHyp and AgPro complex. After the addition of silver(I) complexes the zeta potential of BSA did not show significant changes. All values of $\zeta$ were within the experimental error. These results noticeably indicate that there is no significant structural change on the protein surface upon the binding of the examined complexes.

### Lipophilicity

To evaluate the structural and biological properties of new silver(I) complexes, the $\log P$ partition coefficient was determined by the traditional method of shaking the flask to evaluate the bioavailability of the studied complexes.[74]

The complexes have a hydrophilic feature as the $\log P$ coefficients are negative ($\log P$ (AgPro) = −1.46; $\log P$ (AgHyp) = −1.16). Comparing the above results of biological activity and the $\log P$ value, it is clear that the AgPro complex with its slightly more hydrophilic character shows a slightly higher biological activity than the complex AgHyp (whether antibacterial or anticancer). The $\log P$ partition coefficient was determined for other silver(I) complexes AgGly, AgAla and AgPhe with amino acid ligands glycine, alanine and phenylalanine, respectively[34] and silver(I) complexes AgFu2c and AgPy2c with 5-membered heterocyclic aromatic carboxylate ligands (Fu2c = furan-2-carboxylate; Py2c = pyrrole-2-carboxylate).[75] The values of $\log P$ were negative for all the mentioned complexes and the same trend between these values and the biological activity was observed. The more hydrophilic complexes AgGly ($\log P$ = −2.74) and AgAla ($\log P$ = −2.36) demonstrate a similar higher effect against bacteria and AgPhe ($\log P$ = −0.96) is practically inactive.[34] A similar trend was observed in the case of the silver(I) complexes AgFu2c ($\log P$ = −2.04) and AgPy2c ($\log P$ = −1.44); complex AgFu2c with a more hydrophilic character exhibits higher antibacterial activity. Besides that, other factors probably influence the complexes' ability to suppress microbial growth, as microorganisms were more sensitive to the silver(I) amino acid complexes (*e.g.* for the method and availability of the complexes' transport into cells – amino acid complexes are probably more bioaccessible for transport).[75]

To estimate and correlate the experimentally determined $\log P$ value with the theoretical value, we compared the Gibbs energy of the same particles in both solvents, applying the influence of selected parameters in the chosen model and selected calculation methods. From the thermodynamic point of view, the octanol/water partition coefficient $P$ (eqn (4)) is related to the distribution equilibria of the type (eqn (5)). Thus, the estimated value of $\log P$ is proportional to the free energy change during the process (eqn (5)). For diluted solutions, the activity coefficients can be approximated by unity (therefore, $c \approx a$), (eqn (4) and (6)).

$$P = [\text{Solute}]_{oc}/[\text{Solute}]_{w} \approx a(\text{Solute})_{oc}/a(\text{Solute})_{w} \quad (4)$$

$$\text{Solute(water)} \rightleftarrows \text{Solute(1-octanol)}, \Delta G^{\circ} \quad (5)$$

$$\log P \approx -\Delta G^{\circ}/(2.303RT) \quad (6)$$

**Table 8** Zeta potential ($\zeta$) for BSA in the absence and presence of Ag complexes at 298.15 K in PBS solution (pH 7.4). [BSA] = 1.00 × $10^{-5}$ M and [Ag complex] = 5.83 × $10^{-6}$ M

| Sample | $\zeta$ [mV] | SD |
|---|---|---|
| BSA | −12.53 | ±1.27 |
| AgPro | −11.70 | ±1.40 |
| AgHyp | −13.40 | ±2.26 |

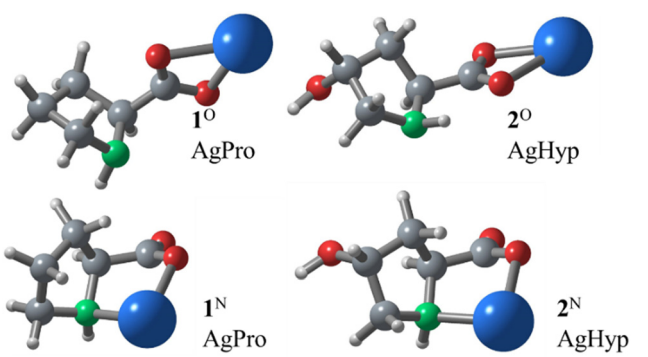


**Fig. 9** Two different optimized structure types predicted for the complexes AgPro and AgHyp in solution state (B3LYP/3-21G, CPCM, water).[76]

Published on 12 April 2024. Downloaded on 3/12/2025 6:23:37 AM.

To elucidate the influence of parameters in the chosen model on the predicted log *P* values, three series differing in the (a) *level of theory*, (b) *basis set*, and (c) *implicit solvation model* type were investigated. Generally, in the case of the studied complexes AgPro and AgHyp, two different types of optimized structure were predicted. The first type (Fig. 9, 1°, 2°) contains the Ag atom bonded to the carboxylate group, making a four-membered ring COAgO. Despite the fact that it is somewhat similar to the motif found in the solid state (Fig. 1 and 2), an alternative structure containing a five-membered ring CCOAgN (Fig. 9, $1^N$, $2^N$) seems to be lower in energy, and its major presence in solutions is therefore favoured. The corresponding equilibria between the isomeric forms ($1° \rightarrow 1^N$, $2° \rightarrow 2^N$) were calculated in both solvents ($\log K^w$ for water and $\log K^{oc}$ for 1-octanol, respectively) and are listed in Tables S8–S10.† This finding agrees with the hypothesis from the previous work.[33] Thus, for the following considerations, the species $1^N$ and $2^N$ are regarded as the only representative and vastly employed entities in the partition equilibria for both phases.

Because each computational method provided results more or less different from the experimentally determined individual values of log *P*, it seems reasonable to take as merit of correct prediction the difference $\Delta_{21}(\log P)$ between the $2^N$ and $1^N$ log *P* values (including the sign) rather than the absolute values, which may be shifted. As the data in Table S9† suggest, there is strong influence of the level of theory used, and the best correlation to the experimental difference $\Delta_{21}(\log P)$ was achieved in the case of the hybrid DFT functionals, namely the original Minnesota M06,[77] followed by the popular 'general-purpose' B3LYP[78] functional. Surprisingly, for almost any other level (from semi-empirical methods xTB/GFN2 and PM7 through a broad variety of *ab initio* methods including Hartree–Fock DFT methods as well as Møller–Plesset perturbation theory), not only large deviations were observed, but even the range was mismatched ($\Delta_{21}(\log P)$ with a negative sign). The introduction of any kind of dispersion or long-range correction seems to be defective, as illustrated in the case of modified BLYP (LC-BLYP) and B3LYP (CAM-B3LYP, GD3) functionals, or the family of wB97 functionals (Table S8†).

Another dimension in the computational results evaluation is represented by the basis set influence (Table S9†). The limitation in this context is represented by the silver(I) ion, for which larger basis sets than double-zeta are not available. Use of a pseudopotential or smaller basis set combined with larger basis sets for the rest of the molecule did not improve the results, as well as tiny bases for the whole system. The best performance was achieved with the 3-21G basis set for all atoms.

The last important factor investigated was type of the implicit solvation model chosen. As seen from Table S10,† the best results were achieved when the COSMO[79] implementation in the PCM[80] framework was used. On the other hand, the integral equation formalism PCM and the SMD performance were poor. The best correlation of the computed difference $\Delta_{21}(\log P)$ in the $2^N$ and $1^N$ log *P* values to the experimentally obtained was achieved using the M06 or B3LYP functional with the 3-21G basis set in the frame of the CPCM solvation model (Fig. 10). Besides the previous computational studies focused on DFT-based octanol–water partition coefficient predictions,[81,82] our current results reveal the limitations in the methodology design due to the present silver(I) atom, which contradicts larger basis sets as well as more specialized functionals (such as M06-2X) utilization.

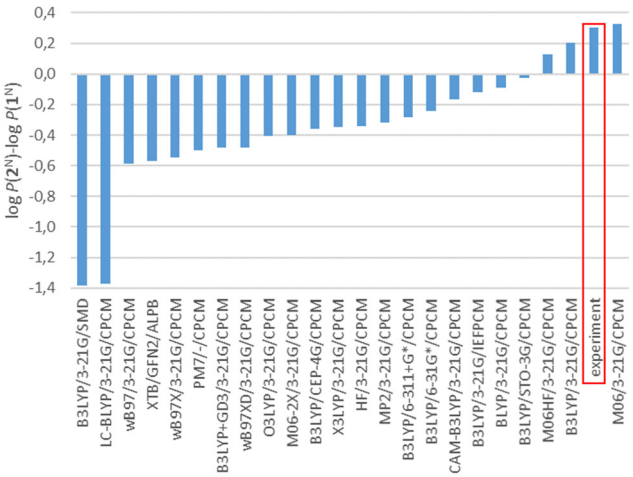


**Fig. 10** Overview of the computational methods and their performance in the correct difference $\Delta_{21}$ (log *P*) values prediction.

## Experimental section

### Materials

L-Proline (Sigma-Aldrich, USA), *trans*-4-hydroxy-L-proline (Acros Organics, Belgium), $AgNO_3$, silver(I) sulfadiazine, 1-octanol (Sigma-Aldrich, USA), *Bacillus cereus* (ATCC 11778 – American Type Culture Collection, USA), *Staphylococcus aureus* (CCM 6188 – Czech Collection of Microorganisms, Czech Republic), *Pseudomonas aeruginosa* (CCM 1960 – Czech Collection of Microorganisms, Czech Republic), Tryptone soya agar (Merck, Germany), filter paper disks, enrofloxacin disk 5 μg (Oxoid, United Kingdom), Tryptone soya broth (Biolife, Italy), 96-well plates (BRANDplates, Germany), Bovine serum albumin BSA (Sigma-Aldrich, USA), dimethylsulfoxide DMSO (Lach-Ner, Czech Republic), dimethylsulfoxide-$d_6$ (Armar Isotopes, Germany), and deuterium oxide (Sigma-Aldrich, USA) were used.

### Synthesis

**Preparation of $\{[Ag_2(Pro)_2(NO_3)]NO_3\}_n$ (AgPro).** Proline (67.7 mg, 0.589 mmol) was dissolved in water (6 mL) and was added into 5 mL of silver(I) nitrate solution (100 mg; 0.589 mmol). The reaction mixture was stirred for 15 min and then allowed to stand in the absence of light. Crystals formed by slow evaporation (1 week) were filtered off and the filtered crystals were dried on filter paper in a Petri dish in the absence of light. Crystals of AgPro complex were used for further characterization. Elemental analysis for AgPro

 This journal is © The Royal Society of Chemistry 2024

Published on 12 April 2024. Downloaded on 3/12/2025 6:23:37 AM.

($C_{10}H_{18}Ag_2N_4O_{10}$): (calcd %): C 21.07; H 3.18; N 9.83. Found: C 21.34; H 3.10; N 9.98. $\Lambda_M$ (DMSO): 43.2 $\Omega^{-1}$ cm$^2$ mol$^{-1}$.

**Preparation of $\{[Ag_2(Hyp)_2(NO_3)]NO_3\}_n$ (AgHyp).** Complex AgHyp was prepared under the same conditions by mixing *trans*-4-hydroxy-L-proline (77.2 mg, 0.589 mmol) and silver(I) nitrate (100 mg; 0.589 mmol) aqueous solutions. Crystals formed by slow evaporation (2 weeks) were also used for further characterization. Elemental analysis for AgHyp ($C_{10}H_{18}Ag_2N_4O_{12}$): (calcd %): C 19.95; H 3.01; N 9.31. Found: C 19.73; H 3.06; N 9.15. $\Lambda_M$ (DMSO): 49.3 $\Omega^{-1}$ cm$^2$ mol$^{-1}$.

## Physical measurements

*Single-crystal diffraction data* for complexes AgPro and AgHyp were collected on a Bruker D8 VENTURE diffractometer using Mo Kα radiation ($\lambda$ = 0.71073 Å). The sample specimens were cooled to 120 K by using an Oxford Cryosystems cooler. Experimental data were processed by the diffractometer software. The structures were solved by direct methods using SHELXT,[83] and the structure models were refined against $F^2$ using SHELXL.[84] All non-hydrogen atoms were refined anisotropically and all hydrogen atoms isotropically. Crystal data are listed in Table S1.† The structure figures were drawn using DIAMOND software.[85]

*Infrared spectra* were recorded on an Avatar FT-IR 6700 (Fourier transform infrared spectroscopy) spectrometer from 4000 to 400 cm$^{-1}$ using an ATR (attenuated total reflectance) technique.

*Elemental analysis* was performed with a CHNOS Elemental Analyzer Vario MICRO from Elementar Analysensysteme GmbH.

*The thermal behaviour* of compounds AgPro and AgHyp was studied by thermogravimetry (TG) using a Setaram Setsys Evolution analyser-1750 under an atmosphere of air. The samples were heated with a heating rate of 10 °C min$^{-1}$ in the temperature range from 25 to 600 °C and with an air flow rate of 60 cm$^3$ min$^{-1}$. Before the thermal measurements, gentle grinding of the samples and careful packing into the corundum crucibles were performed. The mass of samples used in the analyses was within 6–10 mg. The obtained thermoanalytical curves were analysed using the Origin computational program (version 6.1052, Origin Lab Northampton, MA, USA).

*NMR spectra* of AgPro and AgHyp were recorded on a Varian VNMRS (599.87 MHz for $^1$H and 150.84 MHz for $^{13}$C) spectrometer with a 5 mm inverse-detection H–X probe equipped with a *z*-gradient coil at 299.15 K. All the pulse programs were taken from the Varian sequence library. Chemical shifts ($\delta$ in ppm) are given from the internal solvent, and the partially deuterated residual – DMSO-$d_6$ 39.5 ppm for $^{13}$C; DMSO-$d_5$ 2.5 ppm for $^1$H – NMR spectra were processed and analysed in MestReNova 14.3.3 (2023, Mestrelab Research, Spain).

The stability of the silver(I) complexes was recorded on a Varian VNMRS 600 spectrometer operating at 599.87 MHz for $^1$H. The concentration of all the samples was approximately 5 mg per 0.6 mL of 1% DMSO-$d_6$/$D_2O$. The chemical shifts were referenced to the TSP (3-(trimethylsilyl)propionic-2,2,3,3-$d_4$ acid sodium salt) peak ($^1$H NMR 0.00 ppm). All the data were analysed using MestReNova 14.3.3 (2023, Mestrelab Research, Spain) software. The stability of both silver(I) compounds was determined by $^1$H NMR spectroscopy for 4 days.

The molar conductivity of the prepared complexes was measured at room temperature with a Orion Star A212 handheld conductometer using 1.10$^{-3}$ mol dm$^{-3}$ solutions in DMSO.

## Antibacterial activity

**Disk diffusion method.** The antibacterial effect of the new Ag(I) complexes AgPro and AgHyp and the positive control AgSD were evaluated using the disk diffusion method described by Mohamed *et al.*[86] with slight modifications. The antibacterial effect was tested on two G$^+$ bacteria, *Bacillus cereus* (ATCC 11778, USA) and *Staphylococcus aureus* (CCM 6188, Czech Republic), and G$^-$ *Pseudomonas aeruginosa* (CCM 1960, Czech Republic). Bacterial suspensions were prepared in a sterile physiological solution with a density of 0.5 McFarland ($1.5 \times 10^8$ colony forming units (CFU ml$^{-1}$)) and spread out on top of Tryptone soya agar (TSA) in a Petri dish (diameter 90 mm) using a sterile cotton swab. The complexes AgPro and AgHyp were diluted in DMSO + deionized water (the final concentration of DMSO never exceeded 1.0 vol% in the samples). Volumes of 20 µl of the stock solutions of the complexes with a concentration from 0.5 to 0.031 mM were transferred onto sterile filter paper disks (diameter 6 mm) and agar plates were incubated at 30 °C (*Bacillus cereus*) and 37 °C (*Staphylococcus aureus*, *Pseudomonas aeruginosa*) in a thermostat Incucell 111 (BMT a.s., Czech Republic) for 24 hours. The inhibition zone diameter of the growth of the bacteria was measured using a caliper. Samples were tested in duplicate.

**Microdilution method.** The antibacterial activities of Ag(I) complexes – AgPro and AgHyp – and their free ligands – Pro, Hyp – were evaluated using a microdilution method. Also, the activity of the standards as silver(I) nitrate ($AgNO_3$) and silver(I) sulfadiazine (AgSD) was evaluated. The antibacterial effect was tested on two G$^+$ bacteria, *Bacillus cereus* (ATCC 11778, USA) and *Staphylococcus aureus* (CCM 6188, Czech Republic), and G$^-$ *Pseudomonas aeruginosa* (CCM 1960, Czech Republic). The microdilution method was carried out as recommended by CLSI with slight modifications and this method was similarly described by Mohamed *et al.*[86] and Kuchárová *et al.*[87] The complexes were diluted in DMSO + deionized water (the final concentration of DMSO never exceeded 1.0 vol% in the samples). The concentration of the stock solutions of the complexes was in the range from 1 to 0.016 mM. The stock solutions of the samples were two-fold diluted (0.5–0.008 mM) in the wells of a 96-well plate. At first, the wells were filled with 100 µl of Tryptone soya broth (TSB). Then 100 µl of stock solution of the complexes was added to the first well. After mixing, 100 µl of this solution was transferred to the next well, *etc*. Finally, bacterial suspensions were prepared in a sterile physiological solution and 100 µl was transferred into each well with a final density equal to 0.5 McFarland ($1.5 \times 10^8$ colony forming units (CFU ml$^{-1}$)). Samples were tested in triplicate. 96-well plates were incubated at 30 °C (*Bacillus cereus*) and

Published on 12 April 2024. Downloaded on 3/12/2025 6:23:37 AM.

37 °C (*Staphylococcus aureus*, *Pseudomonas aeruginosa*) in a thermostat Incucell 111 (BMT a.s., Czech Republic) for 24 hours. The growth of the bacteria was measured at 600 nm using a Synergy 2 Plate Reader Multi-Mode (BioTek, USA) and evaluated using a statistical method – one way ANOVA, specifically Dunnett's method in GraphPad Prism 6 software. Family-wise alpha threshold and confidence level were 0.05, 95% (confidence interval).

### Cytotoxic activity

**Cell cultures.** The human cancer cell lines HeLa (93021013 ECACC, human cervical adenocarcinoma, United Kingdom), HCT116 (CCL-247™ ATCC, human colorectal carcinoma, USA), A549 (CCL-185™ ATCC, human alveolar adenocarcinoma, USA), A2058 (CRL-3601™ ATCC, human melanoma, USA), PaTu8902 (human pancreatic adenocarcinoma, a gift from Prof. K. Smetana, Institute of Anatomy, Charles University in Prague), HepG2 (HB-8065™ ATCC, human hepatocellular carcinoma, USA) and Jurkat (88042803 ECACC, human leukaemic T cell lymphoma, United Kingdom) were cultured in RPMI 1640 medium (Biosera, Kansas City, MO, USA). MDA-MB-231 (HTB-26™ ATCC, human breast adenocarcinoma, USA) and BJ-5ta (CRL-4001™ ATCC, normal human dermal fibroblasts, USA) cell line were maintained in a growth medium consisting of high-glucose DMEM with sodium pyruvate (Biosera) or DMEM : M199 4 : 1 medium mixture (BJ-5ta cells). Growth medium was supplemented with a 10% fetal bovine serum (FBS, Gibco, Thermo Scientific, Rockford, IL, USA), Antibiotic/Antimycotic Solution (Merck, Darmstadt, Germany) under an atmosphere containing 5% $CO_2$ in humidified air at 37 °C. Cell viability, estimated by trypan exclusion, was greater than 95% before each experiment.

**MTS assay.** The antiproliferative activity of the Ag(I) complexes AgPro and AgHyp, free ligands (Pro, Hyp), $AgNO_3$ and cisplatin was evaluated by colorimetric microculture MTS (3-(4,5-dimethylthiazol-2-yl)-5-(3-carboxymethoxyphenyl)-2-(4-sulfophenyl)-2*H* tetrazolium) assay (Promega, Madison, WI, USA). Cancer cell lines and dermal fibroblasts were seeded at a density of $5 \times 10^3$ cells per well in 96-well polystyrene microplates. Twenty-four hours after cell seeding, different concentrations (10.0–100.0 μM) of the compounds were tested. After 72 hours of incubation, 10 μL of MTS was added to each well. After an additional 2 hours, cell proliferation was evaluated by measuring the absorbance at wavelength 490 nm using the automated Cytation™ 3 Cell Imaging Multi-Mode Reader (Biotek, Winooski, VT, USA). The absorbance of the control wells was taken as 100%, and the results were expressed as a percent of the untreated control. The $IC_{50}$ values were calculated as a predictive TREND model.

### Determination of safety application

Chicken eggs (30 pcs) from the certificate hatchery (Parovske Haje, Nitra, Slovakia) were incubated in an incubator (River ET549/A, River Systems, Italy) with rotation, temperature 37.5 °C and humidity around 60%. Such conditions simulate the normal hatchery process. Before incubation, the eggs were cleaned with water and disinfected with 95% ethanol. At embryonic day one, 3 mL of albumin was extracted by a small hole with a needle. After that, the hole was fixed by liquid paraffin. The eggs were incubated in horizontal position. On the top of the eggs, holes were cut by scissors on embryonic day 8. A disinfected plastic ring was applied to the chorioallantoic membrane. The active substances were diluted in antigen-free phosphate buffer, to eliminate the negative effect of pH, non-isotonic strength, and the irritation effect of other solvents such as distilled water. Isotonic physiological solution (0.9% NaCl) cannot be used, because $Cl^-$ ions should interact with $Ag^+$ ions and form an insoluble precipitate of AgCl. The prepared solutions were transparent, which allowed us to observe their effect on the CAM straight in time. Both samples (AgPro and AgHyp), phosphate buffer (as negative control) and positive controls (1% SDS sodium dodecyl sulphate and 1M NaOH) were tested for irritation potential. The silicone rings with 30 μl of the solution were photographed 0, 30, 120, and 300 seconds after application by a stereomicroscope Olympus SZ61 (Olympus Corporation, Tokyo, Japan), digital camera ARTCAM-300MI (ARTRAY, Tokyo, Japan) and software QuickPhoto 2.3 (PROMICRA, Prague, Czech Republic). The vasoactivity of the substances was evaluated from the photographs by three independent observers to eliminate subjective error. The irritation score was determined by HET-CAM assay using an Irritation Score.[58]

### Fluorescence spectroscopy

The fluorescence spectra were recorded using a Varian Cary Eclipse spectrofluorometer at various temperatures (293.15 K, 298.15 K and 303.15 K) in 10 mM phosphate-buffered saline (pH = 7.4). The spectra were measured at an excitation wavelength of 280 nm (slit width 10 nm for the excitation and emission beams) in the range 300–450 nm. The spectrofluorometric titrations were performed with an increasing concentration of the complexes AgPro and AgHyp. $K_{SV}$ constants were determined according to the classical Stern–Volmer eqn (7) described previously:[88]

$$\frac{F_0}{F} = 1 + K_{SV}\,[Q] \tag{7}$$

where $F_0$ and $F$ are the fluorescence intensities in the absence and the presence of the quencher at 348 nm. $K_{SV}$ is the Stern–Volmer quenching constant and [Q] is the concentration of the quencher.

### Zeta potential analysis

The zeta potential of the BSA in the absence and the presence of complexes AgPro and AgHyp was measured using a Malvern Zetasizer Nano ZS90. BSA was dissolved in 10 mM phosphate-buffered saline (pH = 7.4) and the concentration of the BSA solution was $1.00 \times 10^{-5}$ M. The concentration of silver(I) complexes was $5.83 \times 10^{-6}$ M (the highest concentration used in the fluorescence quenching experiments). The measurements were performed at 298.15 K with 10 runs and the zeta potential was reported as the average of the measurements.


This journal is © The Royal Society of Chemistry 2024

Published on 12 April 2024. Downloaded on 3/12/2025 6:23:37 AM.

### Lipophilicity

The water/1-octanol partition coefficients of AgPro and AgHyp were determined by the shake-flask method according to the OECD guidelines.[74] The silver(I) complexes were dissolved in water, and saturated with 1-octanol with a concentration of stock solutions of $2 \times 10^{-4}$ M. A UV–vis calibration curve was prepared for each complex. Then, equal volumes of silver(I) compound stock solution and water-saturated 1-octanol were mixed for 1 h, the organic and aqueous phases were separated and the concentration of the sample in aqueous solution was determined by UV–vis measurement. Finally, the concentration of the sample in 1-octanol was calculated based on the difference of the concentration of the sample in the stock solution and the concentration in the aqueous phase after shaking, and $P$ values, [sample in octanol]/[sample in water],[68] were determined for each complex. The measurements were performed in duplicate and the results are expressed as the logarithmic partition coefficients ($\log P$).

**Theoretical estimation.** Candidate structures of complexes AgPro and AgHyp employed in the solution state were optimized at various levels of theory, including the modern semi-empirical as well as DFT methods, all in the frame of implicit solvent models. In the part of computations carried out in the Gaussian 16 program package,[53] pure water and pure 1-octanol were chosen as the solvents. On the other hand, pure water and "wet" (water-saturated) 1-octanol were utilized in the frame of the ALPB solvation model when using the semi-empirical xTB code.[47–52] A similar computational protocol was utilized in the case of dimeric structures modelling, for which DMSO was chosen as the solvent (in both programs). The identity of the minima was checked, and no imaginary vibrational frequencies were found.

## Conclusion

Naturally occurring AMPs and ACPs or their synthetically modified analogues appear as potential biocompatible and bioavailable chemotherapeutics of the future. One of the possibilities of their modification is interaction with therapeutically active metal ions. In this work, we presented the influence of Pro and Hyp coordination (as components of AMPs and ACPs) on the biological activity of silver(I) ions. First, we isolated the AgPro and AgHyp complexes in crystalline form, which allowed us to know their exact composition and structure and to correlate their structural properties with spectral and thermal ones in the solid phase. In addition, we confirmed their stability and dimeric complex species presence in the DMSO. From the point of view of their bioassays, we found that the coordination of silver(I) ion by both selected ligands did not significantly influence its antibacterial activity. On the other side, surprisingly, both complexes seem to be more anti-cancer active (compared with their antibacterial activity). Moreover, the complexes' activity against the MDA-MB-231 and Jurkat cancer cell lines is higher and in the case of breast cancer cells even more selective than cisPt. Additionally, *in ovo* tests predict the safe use of the AgPro and AgHyp complexes in case of their topical or intravenous application. From fluorescence measurements at four different temperatures were calculated binding constants which indicate moderate affinities of our complexes for BSA protein binding. The negative values of the thermodynamic parameter $\Delta G$ revealed that the reaction of Ag(I) complexes with BSA proceeds spontaneously. The zeta potential measurements indicated no significant structural changes in plasma protein. Both *in ovo* and fluorescence quenching experiments indicate a suitable bioavailability of the new complexes, while the determined partition coefficient $\log P$ points to the slightly higher hydrophilic character of the AgPro complex and thus its slightly higher bioactivity.

Moreover, from the evaluation of the theoretical approach to the behaviour of our complexes in different solvents (and thus also to their bioavailability), the influence of solvents on the composition and form of complexes in solutions is obvious. While the dimeric form (corresponding to the crystalline form of the complexes) was estimated in pure DMSO, in solutions with a significant excess of water, the presence of complex species with the five-membered CCOAgN ring at a neutral pH (close to physiological conditions) could be preferred. It follows from the above that for correlations of this type it is necessary to obtain a significantly more robust set of experimental data (thermodynamic equilibrium parameters, kinetic stability/lability, *etc.*) to propose a suitable theoretical approach to the SAR (structure–activity relationship) in accordance with the experimental data for silver(I) complexes (probably also for other metal ion complexes). In our opinion, this approach would significantly help in the future in the design of new potentially effective drugs based on metal ion complexes and therefore it is necessary to systematically work on the design, preparation and characterization of bioavailable silver(I) complexes (but also of other metal ions).

## Author contributions

Gabriela Kuzderová prepared and investigated the complexes and contributed to the writing and finalization of the original draft manuscript (investigation, writing – original draft, visualization). Simona Sovová investigated the antibacterial properties and BSA binding properties (investigation, visualization). Michaela Rendošová investigated the complexes' lipophilicity and contributed to the writing of the original draft manuscript (investigation, writing – original draft, visualization). Róbert Gyepes measured and solved the crystal structures of the complexes (investigation). Danica Sabolová designed and supervised the spectral experiments, analysed, interpreted, and validated the data, and also contributed to the original draft manuscript (supervision, validation, writing – original draft, visualization). Ivona Kožárová designed and supervised the antibacterial experiments (supervision, validation). Ľudmila Balážová designed and investigated the *in ovo* experiments and contributed to the writing of original draft manuscript (investigation, validation, writing – original draft, visual-

Published on 12 April 2024. Downloaded on 3/12/2025 6:23:37 AM.

ization). Mária Vilková investigated and validated the NMR spectra and contributed to the writing of the original draft manuscript (investigation, writing – original draft, visualization). Martin Kello designed and supervised the anticancer experiments, analysed and interpreted the data, and performed statistical analyses (investigation, validation). Alan Liška investigated, designed and performed computational methods and contributed to the writing of the original draft manuscript (investigation, methodology, software, writing – original draft, visualization). Zuzana Vargová supervised the students during the complexes' preparation and investigation and is responsible for the idea and concept of the article (conceptualization, methodology, validation, supervision, visualization, writing – original draft, writing – review & editing). All authors have read and agreed to the published version of the manuscript.

## Conflicts of interest

There are no conflicts to declare.

## Acknowledgements

This work was financially supported by Slovak grant agencies VEGA, KEGA and APVV (Scientific Grant Agency, Cultural and Educational Grant Agency of Ministry of Education, Science, Research and Sport of the Slovak Republic and Slovak Research and Development Agency): VEGA 1/0498/23, 1/0037/22, 1/0347/23, 1/0268/24, KEGA 007UPJŠ-4/2024, APVV-20-0073 and VVGS vvgs-2023-2543. The authors are very grateful to Jana Havlíčková for the thermal analysis measurements and Patrícia Hudecová and Simona Hriciková for antibacterial and Simona Žiláková for anticancer measurements. Computational resources were provided by the e-INFRA CZ project (ID: 90254), supported by the Ministry of Education, Youth and Sports of the Czech Republic.

## References

1 J. Xuan, W. Feng, J. Wang, R. Wang, B. Zhang, L. Bo, Z.-S. Chen, H. Yang and L. Sun, *Drug Resistance Updates*, 2023, **68**, 100954.
2 D. W. Hoskin and A. Ramamoorthy, *Biochim. Biophys. Acta, Biomembr.*, 2008, **1778**, 357–375.
3 D. Gaspar, A. S. Veiga and M. A. R. B. Castanho, *Front. Microbiol.: Antimicrob., Resist. Chemother.*, 2013, **4**, 294.
4 A. Tyagi, A. Tuknait, P. Anand, S. Gupta, M. Sharma, D. Mathur, A. Joshi, S. Singh, A. Gautam and G. P. S. Raghava, *Nucleic Acids Res.*, 2015, **43**, 837–843.
5 Y. Qin, Z. D. Qin, J. Chen, C. G. Cai, L. Li, L. Y. Feng, Z. Wang, G. J. Duns, N. Y. He, Z. S. Chen and X. F. Luo, *Recent Pat. Anticancer Drug Discov.*, 2019, **14**, 70–84.
6 Web of Science, Clarivate. **https://www.webofscience.com/wos/woscc/basic-search**, 2024.
7 I. P. Encalada, L. M. C. Cocom, N. C. Q. Bojórquez and M. R. S. Campos, *Int. J. Pept. Res. Ther.*, 2023, **29**, 62.
8 A. L. Lehninger, D. L. Nelson and M. M. Cox, *Principles of Biochemistry (3rd ed.)*, W. H. Freeman, New York, 2000.
9 K. L. Gorres and R. T. Raines, *Crit. Rev. Biochem. Mol. Biol.*, 2010, **45**, 106–124.
10 E. J. Patriarca, F. Cermola, C. D'Aniello, A. Fico, O. Guardiola, D. De Cesare and G. Minchiotti, *Front. Cell Dev. Biol.*, 2021, **9**, 728576.
11 W. Li, J. Tailhades, N. M. O'Brien-Simpson, F. Separovic, L. Otvos, M. A. Hossain and J. D. Wade, *Amino Acids*, 2014, **46**, 2287–2294.
12 A. K. Mishra, J. Choi, E. Moon and K.-H. Baek, *Molecules*, 2018, **23**, 815.
13 R. Sable, P. Parajuli and S. Jois, *Mar. Drugs*, 2017, **15**, 124.
14 J. Bojarska, A. Mieczkowski, Z. M. Ziora, M. Skwarczynski, I. Toth, A. O. Shalash, K. Parang, S. A. El-Mowafi, E. H. M. Mohammed, S. Elnagdy, M. AlKhazindar and W. M. Wolf, *Biomolecules*, 2021, **11**, 1515.
15 C. Di Natale, I. De Benedictis, A. De Benedictis and D. Marasco, *Antibiotics*, 2020, **9**, 337.
16 A. A. Bhat, I. Singh, N. Tandon and R. Tandon, *Eur. J. Med. Chem.*, 2023, **246**, 114954.
17 A. Dobrova, S. Platzer, F. Bacher, M. N. M. Milunovic, A. Dobrov, G. Spengler, É. A. Enyedy, G. Novitchi and V. B. Arion, *Dalton Trans.*, 2016, **45**, 13427–13439.
18 C. I. Diakos, M. Zhang, P. J. Beale, R. R. Fenton and T. W. Hambley, *Eur. J. Med. Chem.*, 2009, **44**, 2807–2814.
19 T. Q. Abd Alkareem and E. J. Waheed, *Chem. Methodol.*, 2022, **6**, 914–928.
20 M. Nath, P. Roy, R. Mishra and M. Thakur, *Appl. Organomet. Chem.*, 2019, **33**, e4663.
21 C. R. Groom, I. J. Bruno, M. P. Lightfoot and S. C. Ward, *Acta Crystallogr., Sect. B: Struct. Sci.*, 2016, **72**, 171–179.
22 E. A. Mikhalyova, S. V. Kolotilov, O. Cador, F. Pointillart, S. Golhen, L. Ouahab and V. V. Pavlishchuk, *Inorg. Chim. Acta*, 2010, **363**, 3453–3460.
23 R. P. Sartoris, L. Ortigoza, N. M. C. Casado, R. Calvo, E. E. Castellano and O. E. Piro, *Inorg. Chem.*, 1999, **38**, 3598–3604.
24 Y. Yukawa, *J. Chem. Soc., Dalton Trans.*, 1992, 3217–3221.
25 G. Venkatesan, G. Anandha Babu, P. Ramasamy and A. Chandramohan, *J. Mol. Struct.*, 2013, **1033**, 121–126.
26 D. B. Hobart, Jr., J. S. Merola, H. M. Rogers, S. Sahgal, J. Mitchell, J. Florio and J. W. Merola, *Catalysts*, 2019, **9**, 515.
27 R. I. Yousef, M. Bette, G. N. Kaluđerović, R. Paschke, C. Yiran, D. Steinborn and H. Schmidt, *Polyhedron*, 2011, **30**, 1990–1996.
28 L. Yang, D. R. Powell and R. P. Houser, *Dalton Trans.*, 2007, 955–964.
29 Y. Zorlu, H. Can and F. Aksakal, *J. Mol. Struct.*, 2013, **1049**, 368–376.
30 Y. Yukawa, Y. Inomata and T. Takeuchi, *Bull. Chem. Soc. Jpn.*, 1983, **56**, 2125–2128.
31 N. C. Kasuga, R. Yamamoto, A. Hara, A. Amano and K. Nomiya, *Inorg. Chim. Acta*, 2006, **359**, 4412–4416.


This journal is © The Royal Society of Chemistry 2024

Published on 12 April 2024. Downloaded on 3/12/2025 6:23:37 AM.

32 K. Nomiya and H. Yokoyama, *J. Chem. Soc., Dalton Trans.*, 2002, 2483–2490.
33 M. Rendošová, Z. Vargová, J. Kuchár, D. Sabolová, Š. Levoča, J. Kudláčová, H. Paulíková, D. Hudecová, V. Helebrandtová, M. Almáši, M. Vilková, M. Dušek and D. Bobáľová, *J. Inorg. Biochem.*, 2017, **168**, 1–12.
34 G. Kuzderová, M. Rendošová, R. Gyepes, M. Almáši, D. Sabolová, M. Vilková, P. Olejníková, D. Hudecová, M. Kello and Z. Vargová, *J. Inorg. Biochem.*, 2020, **210**, 111170.
35 M. Rendošová, R. Gyepes, I. C. Maruščáková, D. Mudroňová, D. Sabolová, M. Kello, M. Vilková, M. Almáši, V. Huntošová, O. Zemek and Z. Vargová, *Dalton Trans.*, 2021, **50**, 936–953.
36 H. Schmidbaur and A. Schier, *Angew. Chem., Int. Ed.*, 2015, **54**, 746–784.
37 K. F. Baranova, A. A. Titov, O. A. Filippov, A. F. Smol'yakov, A. A. Averin and E. S. Shubina, *Crystals*, 2020, **10**, 881.
38 K. M. Priyadarshini, A. Chandramohan, G. A. Babu and P. Ramasamy, *Optik*, 2014, **125**, 1390–1395.
39 Y. S. Mary, L. Ushakumari, B. Harikumar, H. T. Varghese and C. Y. Panicker, *J. Iran. Chem. Soc.*, 2009, **6**, 138–144.
40 R. V. Rajan, L. K. Joy, D. Sajan, A. K. Thomas, S. Sathiskumar, T. Balakrishnan and G. Vinitha, *J. Mol. Struct.*, 2020, **1204**, 127457.
41 S. M. Soliman, R. Assem, M. A. M. Abu-Youssef and T. S. Kassem, *J. Mol. Struct.*, 2015, **1085**, 126–136.
42 Z. Rzączyńska, R. Mrozek and T. Glowiak, *J. Chem. Crystallogr.*, 1997, **27**, 417–422.
43 A. S. Potapov, E. A. Nudnova, A. I. Khlebnikov, V. D. Ogorodnikov and T. V. Petrenko, *Inorg. Chem. Commun.*, 2015, **53**, 72–75.
44 K. Boopathi and P. Ramasamy, *J. Mol. Struct.*, 2015, **1080**, 37–43.
45 K. Boopathi, S. M. Babu, R. Jagan, S. Athimoolam and P. Ramasamy, *New J. Chem.*, 2018, **42**, 17464–17477.
46 T. P. Andrejević, D. Milivojevic, B. Đ. Glišić, J. Kljun, N. L. Stevanović, S. Vojnovic, S. Medic, J. Nikodinovic-Runic, I. Turel and M. I. Djuran, *Dalton Trans.*, 2020, **49**, 6084–6096.
47 C. Bannwarth, E. Caldeweyher, S. Ehlert, A. Hansen, P. Pracht, J. Seibert, S. Spicher and S. Grimme, *Wiley Interdiscip. Rev.: Comput. Mol. Sci.*, 2020, **11**, 04193.
48 C. Bannwarth, S. Ehlert and S. Grimme, *J. Chem. Theory Comput.*, 2019, **15**, 1652–1671.
49 S. Ehlert, M. Stahn, S. Spicher and S. Grimme, *J. Chem. Theory Comput.*, 2021, **17**, 4250–4261.
50 E. Caldeweyher, C. Bannwarth and S. Grimme, *J. Chem. Phys.*, 2017, **147**, 034112.
51 E. Caldeweyher, S. Ehlert, A. Hansen, H. Neugebauer, S. Spicher, C. Bannwarth and S. Grimme, *J. Chem. Phys.*, 2019, **150**, 154122.
52 E. Caldeweyher, J.-M. Mewes, S. Ehlert and S. Grimme, *Phys. Chem. Chem. Phys.*, 2020, **22**, 8499–8512.
53 M. J. Frisch, G. W. Trucks, H. B. Schlegel, G. E. Scuseria, M. A. Robb, J. R. Cheeseman, G. Scalmani, V. Barone, G. A. Petersson, H. Nakatsuji, X. Li, M. Caricato, A. V. Marenich, J. Bloino, B. G. Janesko, R. Gomperts, B. Mennucci, H. P. Hratchian, J. V. Ortiz, A. F. Izmaylov, J. L. Sonnenberg, D. Williams-Young, F. Ding, F. Lipparini, F. Egidi, J. Goings, B. Peng, A. Petrone, T. Henderson, D. Ranasinghe, V. G. Zakrzewski, J. Gao, N. Rega, G. Zheng, W. Liang, M. Hada, M. Ehara, K. Toyota, R. Fukuda, J. Hasegawa, M. Ishida, T. Nakajima, Y. Honda, O. Kitao, H. Nakai, T. Vreven, K. Throssell, J. A. Montgomery, Jr., J. E. Peralta, F. Ogliaro, M. J. Bearpark, J. J. Heyd, E. N. Brothers, K. N. Kudin, V. N. Staroverov, T. A. Keith, R. Kobayashi, J. Normand, K. Raghavachari, A. P. Rendell, J. C. Burant, S. S. Iyengar, J. Tomasi, M. Cossi, J. M. Millam, M. Klene, C. Adamo, R. Cammi, J. W. Ochterski, R. L. Martin, K. Morokuma, O. Farkas, J. B. Foresman and D. J. Fox, *Gaussian 16, Revision C.01*, Gaussian, Inc., Wallingford CT, 2016.
54 Z. Vargová, P. Olejníková, G. Kuzderová, M. Rendošová, J. Havlíčková, R. Gyepes and M. Vilková, *Bioorg. Chem.*, 2023, **141**, 106907.
55 J. S. Glasser, C. H. Guymon, K. Mende, S. E. Wolf, D. R. Hospenthal and C. K. Murray, *Burns*, 2010, **36**, 1172–1184.
56 V. C. Brenner and J. C. Sherris, *Antimicrob. Agents Chemother.*, 1972, **1**, 116–122.
57 E. J. Kay, S. Zanivan and A. Rufini, *Curr. Opin. Biotechnol.*, 2023, **84**, 103011.
58 N. P. Luepke, *Food Chem. Toxicol.*, 1985, **23**, 287–291.
59 R. H. F. Costa, A. P. Krawczyk-Santos, J. F. Martins Andrade, G. N. Barbalho, R. M. Almeida, Y. K. M. Nóbrega, M. Cunha-Filho, G. M. Gelfuso, S. F. Taveira and T. Gratieri, *Carbohydr. Polym.*, 2023, **302**, 120420.
60 H. Spielmann, M. Liebsch, S. Kalweit, F. Moldenhauer, T. Wirnsberger, H.-G. Holzhütter, B. Schneider, S. Glaser, I. Gerner, W. J. W. Pape, R. Kreiling, K. Krauser, H. G. Miltenburger, W. Steiling, N. P. Luepke, N. Müller, H. Kreuzer, P. Mürmann, J. Spengler, E. Bertram-Neis, B. Siegemund and F. J. Wiebel, *Altern. Lab. Anim.*, 1996, **24**, 741–858.
61 W. Steiling, M. Bracher, P. Courtellemont and O. de Silva, *Toxicol. in Vitro*, 1999, **13**, 375–384.
62 D. Ribatti, *Mech. Dev.*, 2016, **141**, 70–77.
63 R. Palmeira-de-Oliveira, R. M. Machado, J. Martinez-De-Oliveira and A. Palmeira-de-Oliveira, *ALTEX*, 2018, **35**, 495–503.
64 A. Batista-Duharte, G. Jorge Murillo, U. M. Pérez, E. N. Tur, D. F. Portuondo, B. T. Martínez, D. Téllez-Martínez, J. E. Betancourt and O. Pérez, *Int. J. Toxicol.*, 2016, **35**, 627–633.
65 J. E. Dahl, *Acta Odontol. Scand.*, 2007, **65**, 275–283.
66 V. Díaz-Tomé, C. Bendicho-Lavilla, X. García-Otero, R. Varela-Fernández, M. Martín-Pastor, J. Llovo-Taboada, P. Alonso-Alonso, P. Aguiar, M. González-Barcia, A. Fernández-Ferreiro and F. J. Otero-Espinar, *Pharmaceutics*, 2023, **15**, 35.

Published on 12 April 2024. Downloaded on 3/12/2025 6:23:37 AM.

67 J. H. Draize, G. Woodard and H. O. Calvery, *J. Pharmacol. Exp. Ther.*, 1944, **82**, 377–390.
68 J. Scheel, M. Kleber, J. Kreutz, E. Lehringer, A. Mehling, K. Reisinger and W. Steiling, *Regul. Toxicol. Pharmacol.*, 2011, **59**, 471–492.
69 S. Naveenraj and S. Anandan, *J. Photochem. Photobiol., C*, 2013, **14**, 53–71.
70 J. Shi, D. Pan, M. Jiang, T. T. Liu and Q. Wang, *J. Photochem. Photobiol., B*, 2016, **164**, 103–111.
71 S. Roy, R. K. Nandi, S. Ganai, K. C. Majumdar and T. K. Das, *J. Pharm. Anal.*, 2017, **7**, 19–26.
72 V. D. Suryawanshi, L. S. Walekar, A. H. Gore, P. V. Anbhule and G. B. Kolekar, *J. Pharm. Anal.*, 2016, **6**, 56–63.
73 O. A. Chaves, B. Mathew, D. Cesarin-Sobrinho, B. Lakshminarayanan, M. Joy, G. E. Mathew, J. Suresh and J. C. Netto-Ferreira, *J. Mol. Liq.*, 2017, **242**, 1018–1026.
74 Test No. 107: Partition Coefficient (n-octanol/water): Shake Flask Method, **https://www.oecd-ilibrary.org/environment/test-no-107-partition-coefficient-n-octanol-water-shake-flask-method_9789264069626-en**.
75 M. Rendošová, R. Gyepes, M. Kello, M. Vilková, D. Mudroňová, P. Olejníková, P. Cardiano, S. Gama, D. Milea and Z. Vargová, *J. Inorg. Biochem.*, 2023, **246**, 112266.
76 Y. Podolyan and J. Leszczynski, *Int. J. Quantum Chem.*, 2009, **109**, 8–16.
77 Y. Zhao and D. G. Truhlar, *Theor. Chem. Acc.*, 2008, **120**, 215–241.
78 A. D. Becke, *J. Chem. Phys.*, 1993, **98**, 5648–5652.
79 A. Klamt and G. Schüürmann, *J. Chem. Soc., Perkin Trans. 2*, 1993, 799–805.
80 C. Amovilli, V. Barone, R. Cammi, E. Cancès, M. Cossi, B. Mennucci, C. S. Pomelli and J. Tomasi, *Adv. Quantum Chem.*, 1998, **32**, 227–261.
81 L. Saranjam, E. Fuguet, M. Nedyalkova, V. Simeonov, F. Mas and S. Madurga, *Symmetry*, 2021, **13**, 1750.
82 M. A. Nedyalkova, S. Madurga, M. Tobiszewski and V. Simeonov, *J. Chem. Inf. Model.*, 2019, **59**, 2257–2263.
83 G. M. Sheldrick, *Acta Crystallogr., Sect. A: Found. Adv.*, 2015, **71**, 3–8.
84 G. M. Sheldrick, *Acta Crystallogr., Sect. C: Struct. Chem.*, 2015, **71**, 3–8.
85 K. Brandenburg and H. Putz, *DIAMOND–Crystal and Molecular Structure Visualization, v6.3*, Crystal Impact GbR, Bonn, 2020.
86 E. H. Mohamed, Y. S. Alghamdi, S. Mostafa Abdel-Hafez, M. M. Soliman, S. H. Alotaibi, M. Y. Hassan, N. A.-D. Hany and H. H. Amer, *Dose-Response*, 2020, **18**, 155932582093618.
87 V. Kuchárová, J. Kuchár, A. Lüköová, R. Jendželovský, M. Majerník, P. Fedoročko, M. Vilková, I. D. Radojević, L. R. Čomić and I. Potočňák, *Polyhedron*, 2019, **170**, 447–457.
88 G. Kuzderová, M. Rendošová, R. Gyepes, S. Sovová, D. Sabolová, M. Vilková, P. Olejníková, I. Bačová, S. Stokič, M. Kello and Z. Vargová, *Molecules*, 2021, **26**, 6335.


This journal is © The Royal Society of Chemistry 2024